Ketogenesis mitigates metabolic dysfunction-associated steatotic liver disease through mechanisms that extend beyond fat oxidation

Eric D. Queathem, … , Patrycja Puchalska, Peter A. Crawford

Research In-Press Preview **Hepatology** **Metabolism**

The progression of metabolic dysfunction-associated steatotic liver disease (MASLD) to metabolic dysfunction-associated steatohepatitis (MASH) involves alterations in both liver-autonomous and systemic metabolism that influence the liver's balance of fat accretion and disposal. Here, we quantify the contributions of hepatic oxidative pathways to liver injury in MASLD-MASH. Using NMR spectroscopy, UHPLC-MS, and GC-MS, we performed stable-isotope tracing and formal flux modeling to quantify hepatic oxidative fluxes in humans across the spectrum of MASLD-MASH, and in mouse models of impaired ketogenesis. In humans with MASH, liver injury correlated positively with ketogenesis and total fat oxidation, but not with turnover of the tricarboxylic acid cycle. Loss-of-function mouse models demonstrated that disruption of mitochondrial HMG-CoA synthase (HMGCS2), the rate-limiting step of ketogenesis, impairs overall hepatic fat oxidation and induces a MASLD-MASH-like phenotype. Disruption of mitochondrial β-hydroxybutyrate dehydrogenase (BDH1), the terminal step of ketogenesis, also impaired fat oxidation, but surprisingly did not exacerbate steatotic liver injury. Taken together, these findings suggest that quantifiable variations in overall hepatic fat oxidation may not be a primary determinant of MASLD-to-MASH progression, but rather, that maintenance of ketogenesis could serve a protective role through additional mechanisms that extend beyond overall rates of fat oxidation.

Find the latest version:

https://jci.me/191021/pdf

1 **Ketogenesis mitigates metabolic dysfunction-associated steatotic liver disease through**

2 **mechanisms that extend beyond fat oxidation**

3 Eric D. Queathem[1,2,3], David B. Stagg[1], Alisa B. Nelson[1], Alec B. Chaves[4], Scott B. Crown[4], Kyle

4 Fulghum[1], D. Andre d'Avignon[1], Justin R. Ryder[5], Patrick J. Bolan[6], Abdirahman Hayir[1], Jacob

5 R. Gillingham[1,2], Shannon Jannatpour[7], Ferrol I. Rome[1], Ashley S. Williams[4], Deborah M.

6 Muoio[4,8,9], Sayeed Ikramuddin[7], Curtis C. Hughey[1], Patrycja Puchalska[1*], Peter A. Crawford[1,2*]

7 [1]Division of Molecular Medicine, Department of Medicine, University of Minnesota Medical

8 School, Minneapolis, MN, USA

9 [2]Department of Biochemistry, Molecular Biology and Biophysics, University of Minnesota

10 Medical School, Minneapolis, MN, USA

11 [3]Department of Integrative Biology and Physiology, University of Minnesota Medical School,

12 Minneapolis, MN, USA

13 [4]Duke Molecular Physiology Institute and Sarah W. Stedman Nutrition and Metabolism Center,

14 Duke University Medical Center, Durham, NC, USA

15 [5]Department of Surgery, Lurie Children's Hospital, Chicago, IL, USA

16 [6]Department of Radiology, University of Minnesota Medical School, Minneapolis, MN, USA

17 [7]Department of Surgery, University of Minnesota, Minneapolis, MN, USA

18 [8]Division of Endocrinology, Metabolism, and Nutrition, Department of Medicine, Duke University

19 Medical Center, Durham, NC, USA

20 [9]Department of Pharmacology and Cancer Biology, Duke University Medical Center, Durham,

21 NC, USA

22 *Contact for correspondence, crawforp@umn.edu or ppuchals@umn.edu
23 Address: 425 E. River Pkwy, Dwan Bldg, Minneapolis, MN, 55455-0368
24 Phone number: +1 612-301-2202

27   **Abstract**

28   The progression of metabolic dysfunction-associated steatotic liver disease (MASLD) to

29   metabolic dysfunction-associated steatohepatitis (MASH) involves alterations in both liver-

30   autonomous and systemic metabolism that influence the liver's balance of fat accretion and

31   disposal. Here, we quantify the contributions of hepatic oxidative pathways to liver injury in

32   MASLD-MASH. Using NMR spectroscopy, UHPLC-MS, and GC-MS, we performed stable-

33   isotope tracing and formal flux modeling to quantify hepatic oxidative fluxes in humans across

34   the spectrum of MASLD-MASH, and in mouse models of impaired ketogenesis. In humans with

35   MASH, liver injury correlated positively with ketogenesis and total fat oxidation, but not with

36   turnover of the tricarboxylic acid cycle. Loss-of-function mouse models demonstrated that

37   disruption of mitochondrial HMG-CoA synthase (HMGCS2), the rate-limiting step of

38   ketogenesis, impairs overall hepatic fat oxidation and induces a MASLD-MASH-like phenotype.

39   Disruption of mitochondrial β-hydroxybutyrate dehydrogenase (BDH1), the terminal step of

40   ketogenesis, also impaired fat oxidation, but surprisingly did not exacerbate steatotic liver injury.

41   Taken together, these findings suggest that quantifiable variations in overall hepatic fat

42   oxidation may not be a primary determinant of MASLD-to-MASH progression, but rather, that

43   maintenance of ketogenesis could serve a protective role through additional mechanisms that

44   extend beyond overall rates of fat oxidation.

45   **Keywords**

48

49

50

Introduction

The global prevalence of metabolic dysfunction-associated steatotic liver disease (MASLD) is surging and is associated with mortality and multiple comorbidities (1, 2). The natural history of MASLD is tightly linked to obesity and insulin resistance, and involves both liver-autonomous and systemic metabolic abnormalities that drive the ectopic storage of triacylglycerol (TAG) species in hepatocytes (i.e., hepatic steatosis) which is strongly associated with cellular injury, inflammation, and the development of metabolic dysfunction-associated steatohepatitis (MASH), a progressive fibrotic liver disease that markedly increases the risks of cirrhosis and hepatocellular carcinoma (3–5). While the severity of hepatic steatosis correlates with the extent of liver injury, the pathogenesis of MASLD-MASH progresses through multiple parallel and mutually amplifying pathways. For any degree of steatosis, the development of MASH is marked by the appearance of oxidative and inflammatory stress, coupled to hepatocellular injury (i.e., hepatocyte ballooning) which collectively is quantified using the NAFLD (corresponding to the prior term referencing MASLD, nonalcoholic fatty liver disease) activity score (NAS), a histological scoring system ranging 0-8, which encompasses steatosis (0-3), inflammation (0-3) and hepatocyte ballooning (0-2). MASH is defined as a NAS score ≥ 4, and typically coincides with fibrosis, though fibrosis is not included when calculating NAS (6).

Currently there is only one FDA approved drug available for the treatment of MASLD-MASH, while several others have failed due to poor efficacy and/or toxicity, illustrating a need to understand the drivers of hepatic fat accumulation, and the mechanistic link this has to the development of injury and advanced liver disease (7, 8). Though incretin mimetics and sodium-glucose cotransporter 2 (SGLT2) inhibitors show promise for MASLD, approaches that (i) are liver-specific, indicated for patients without diabetes or obesity, (ii) limit lifelong high-cost pharmacotherapy, and/or (iii) limit toxicities, remain an unmet need (9, 10). Prior studies have correlated liver TAGs in obesity and/or MASLD to a rise in hepatic de novo lipogenesis (DNL)

76 (11–16), a diminution in polyunsaturated fatty acids (PUFAs) (17–21), and an acceleration in

77 hepatic oxidative fluxes (22–25). Other studies have shown no changes in hepatic fat oxidation

78 (26–29), or have reported impairments in oxidative metabolism (30–34). Therefore, the lack of

79 consensus regarding alterations in hepatic oxidative fluxes throughout the natural history of

80 MASLD-MASH illustrates one of the key obstacles in developing effective therapeutics.

81   Oxidative metabolism in the liver yields reducing equivalents (REs) in the forms of

82 reduced nicotinamide adenine dinucleotide (NADH) and flavin adenine dinucleotide ($FADH_2$),

83 which are primarily sourced from hepatic fat oxidation via (1) β-oxidation, which generates

84 acetyl-CoA, and (2) terminal oxidation of acetyl-CoA in the tricarboxylic acid (TCA) cycle (35).

85 RE production is also directly coupled to ATP production, which fuels phosphoenolpyruvate

86 (PEP)-derived gluconeogenesis (GNG) via the non-oxidative entry (anaplerosis) and exit

87 (cataplerosis) of intermediates through the TCA cycle (36). In both human and rodent models of

88 MASLD, hepatic TCA cycle turnover and PEP-derived GNG are increased relative to controls

89 (25, 36, 37). Very low density lipoprotein (VLDL) secretion rises with fasting and early in the

90 natural history of steatotic liver disease (38, 39). However, VLDL secretion rates fail to

91 compensate for TAG accumulation with progressive MASLD, and VLDL secretion is intrinsically

92 impaired in humans harboring the PNPLA3 I148M mutation (40–42). While the stimulation of fat

93 disposal pathways may offload excess TAGs, the rise in lipid disposal is insufficient to

94 compensate for the rate of lipid appearance, leading to ectopic fat accumulation and

95 predisposition to injury. In addition to VLDL secretion and terminal oxidation in the TCA cycle,

96 ketogenesis, which produces D-beta-hydroxybutyrate (D-βOHB) and acetoacetate (AcAc), is a

97 major conduit supporting hepatic fat disposal. Congenital deficiency of the fate-committing

98 enzyme of ketogenesis, 3-hydroxymethylglutaryl-CoA (HMG-CoA) synthase 2 (HMGCS2), is

99 linked to hepatomegaly and steatosis (43, 44). Moreover, programmed ketogenic insufficiency in

100 mice is associated with more aggressive MASLD progression (45–49). However, the relative

101   rate of ketogenesis in MASLD, compared to controls, has varied among studies (22, 27, 34, 37,

102   50). As such, whether alterations in ketogenesis in human MASLD-MASH play driver,

103   bystander, or compensating roles is debated, as are the mechanisms that link ketogenesis to

104   oxidative metabolism and liver injury. To date, in vivo hepatic oxidative fluxes have only been

105   quantified in humans with uncomplicated MASLD, but have not been measured in humans with

106   histologically-confirmed MASH. To understand the drivers and/or predictors of MASLD-MASH

107   development, progression, and resolution, we quantified hepatic oxidative fluxes in

108   histologically-confirmed MASH patients using nuclear magnetic resonance (NMR) spectroscopy,

109   ultra-high performance liquid chromatography coupled to mass spectrometry (UHPLC-MS), and

110    $^2H/^{13}C$ stable isotope tracing. Ketogenesis insufficient mouse models were used to determine

111   the relationships among ketogenesis, the rate of overall fat oxidation, and liver injury. Together,

112   our observations are consistent with the notion that while ketogenesis and fat oxidation are key

113   inputs into the liver's balance of lipid accretion and disposal, the driver role ketogenesis plays in

114   the rate of hepatic fat oxidation may not be the only determinant of MASLD-to-MASH

115   progression. Therefore, maintenance of hepatic ketogenesis could serve additional protective

116   roles through mechanisms extending beyond its contribution to the rate of hepatic fat oxidation.

117

118

119

120

121

122

123

124 **Results**

125 ***Hepatic ketogenesis correlates with NAS in humans.*** During the progression of MASLD,

126 reports of hepatic oxidative fluxes have been varied, with studies reporting (i) accelerations (22–

127 25), (ii) no changes (26–29), or (iii) impairments (30–34) in oxidative metabolism. However,

128 oxidative fluxes have never been quantified in vivo in humans with histologically-confirmed

129 MASH **(Figure 1A).** To study hepatic metabolism in humans with MASH, participants were

130 recruited from two clinical trials, NCT03997422 and NCT03587831 (**Supplemental Table 1**).

131 Recruited participants remained weight stable during metabolic assessments. Participants with

132 BMI ≥ 35 were screened with magnetic resonance imaging (MRI) to identify patients with a liver

133 proton density fat fraction (PDFF) > 5%, indicative of hepatic steatosis, and a total of 16

134 participants (15 female and 1 male) were recruited to the study outlined in **Figure 1B.** After liver

135 biopsy, glucose homeostasis and body composition were quantified using a frequently sampled

136 intravenous glucose tolerance test (FSIVGTT), and dual-energy X-ray absorptiometry (DXA),

137 respectively. The cohort's characteristics are summarized in **Table** 1. During a 20h fast, oral

138 ^2H_2O and [U-$^{13}C_3$]propionate tracers were delivered to enrich plasma glucose across hydrogen

139 and carbon atoms, whose positional isotopomeric labeling distribution supports modeling of

140 relative reaction velocities (V) (i.e., flux) through hepatic intermediary metabolic pathways.

141 Simultaneously, the absolute rates of endogenous glucose production (EGP) (V_{EGP}) and

142 ketogenesis ($V_{Ra\beta OHB}$) were measured at metabolic and isotopic steady state after a 2h infusion

143 of [3,4-$^{13}C_2$]glucose and D-[U-$^{13}C_4$]βOHB, respectively, thereby allowing the absolute rates of

144 hepatic intermediary metabolic pathways to be quantified **(Supplemental Figure 1)** (35, 51–53).

145 During the screening phase, and prior to flux assessments, a liver biopsy was collected and

146 used to histologically grade liver health, which was collectively summarized by the NAS score.

147 NAS scores ranged from 1-8, all patients exhibited histological signs of steatosis, and 14 out of

148 16 participants displayed signs of hepatocyte cell injury (i.e., ballooning) and/or lobular

149   inflammation **(Figure 1C).** Ten of the 16 participants exhibited histopathological fibrosis. As

150   expected, NAS strongly correlated with PDFF (r = 0.68, P value < 0.01) and liver fibrosis (r =

151   0.79, P value < 0.001) **(Figure 1D)**, but did not correlate with BMI **(Supplemental Figure 2A).**

152   NAS correlated with the acute insulin response to glucose (AIRg) (r = 0.68, P value = 0.005),

153   suggestive of a correlation between insulin resistance and NAS **(Supplemental Figure 2B)**,

154   however, NAS did not correlate with the homeostatic model assessment for insulin resistance

155   (HOMA-IR) **(Supplemental Figure 2C).**

156   We then examined the metabolic flux modeling data acquired in this cohort **(Figure 2A-**

157   **B)**. Across participants, 29 ± 8% of V_{EGP} arose from glycogenolysis ($V_{Glycogen}$), 18 ± 7% from

158   glycerol ($V_{Glycerol}$) and 52 ± 7% from PEP (V_{PEP}) **(Figure 2C).** Next, by quantifying rates of (i)

159   TCA cycle flux, V_{CS}, (ii) total ketone body (TKB) production, V_{RaTKB}, and (iii) GNG sourcing

160   pathways, $V_{Glycerol}$ and V_{PEP}, both hepatic fat oxidation and RE production were calculated. The

161   majority of REs produced in the fasted liver originated from β-oxidation, accounting for 52 ± 15

162   μmol REs/min/kg-lean body mass (LBM), while REs derived from the TCA cycle accounted for

163   33 ± 11 μmol REs/min/kg-LBM, and GNG accounted for 4 ± 3 μmol REs/min/kg-LBM **(Figure**

164   **2D)**. To determine relationships among fluxes, we performed regression analyses and obtained

165   Pearson correlation coefficients **(Supplemental Figure 3A)**. As expected, V_{EGP} correlated with

166    $V_{Glycogen}$, $V_{PEP},$ and total anaplerosis, V_{PEPCK}. Moreover, expected correlations among V_{PEPCK} and

167   pyruvate cycling, V_{PK+ME} (r = 0.99, P value < 0.0001), V_{CS} and V_{PK+ME} (r = 0.60, P value = 0.014),

168   and V_{CS} and V_{PEPCK} (r = 0.65, P value = 0.006) were observed **(Supplemental Figure 3B)**.

169   Additional correlations were observed between V_{EGP} and V_{PK+ME} (r = 0.63, P value = 0.009), V_{EGP}

170   and V_{PEPCK} (r = 0.70, P value = 0.003),, and V_{EGP} and V_{CS} (r = 0.57, P value = 0.020)

171   **(Supplemental Figure 3C)**, as well as V_{PEP} and V_{PK+ME} (r = 0.68, P value = 0.004), V_{PEP} and

172   V_{PEPCK} (r = 0.79, P value < 0.001), and V_{PEP} and V_{CS} (r = 0.68, P value = 0.004) **(Supplemental**

173   **Figure 3D)**. Inverse correlations were observed between the percentage of V_{EGP} attributable to

174   glycerol ($V_{Glycerol}$) and V_{PK+ME}, $V_{PEPCK,}$ and V_{CS} **(Supplemental Figure 3E)**. No correlations were

175   observed between the ketogenic flux $V_{Ra\beta OHB}$ and any individual flux **(Supplemental Figure 3A)**.

176   As expected, total hepatic ketogenesis (V_{RaTKB}) correlated with total hepatic fat oxidation (r =

177   0.96, P value < 0.001), suggesting a driver role of ketogenesis in determining overall rates of

178   hepatic fat oxidation **(Supplemental Figure 3F)**. Interestingly, total fat oxidation was not

179   correlated with V_{CS} (r = 0.22, P value = 0.413) **(Supplemental Figure 3G)**. Taken together,

180   these data reflect internal consistency in the modeling data, demonstrating expected

181   relationships between TCA cycle flux, GNG, ketogenesis, and total fat oxidation.

182   Given the validity of the flux modeling data, we next sought to determine the

183   relationships among these measured fluxes and MASLD-MASH progression. Surprisingly,

184   despite the known relationship among insulin resistance, V_{EGP}, and NAS, a correlation between

185   V_{EGP} and NAS was not detected (r = 0.13, P value = 0.639) **(Figure 2E)**. Moreover, V_{CS},

186     $V_{Glycogen}$, $V_{Glycerol}$, V_{PEP}, V_{PK+ME}, and V_{PEPCK} all showed no correlation with NAS **(Figures 2F,**

187   **Supplemental Figure 4A-B)**. However, surrogates for ketogenesis correlated directly with NAS

188   [$V_{Ra\beta OHB}$ (r = 0.61, P value = 0.013) **Figure 3A**, V_{RaAcAc} (r = 0.58, P value = 0.018), V_{RaTKB} (r =

189   0.61, P value = 0.013), and serum total [^{12}C]ketone bodies (r = 0.53, P value = 0.037),

190   **Supplemental Figure 4C**]. Consistent with the correlation between ketogenesis and total fat

191   oxidation **(Supplemental Figure 3F),** both total fat oxidation (r = 0.63, P value = 0.009) and

192   total RE production (r = 0.52, P value = 0.038) also correlated directly with NAS (**Figure 3B-C**).

193   The mitochondrial redox ratio of βOHB:AcAc did not correlate with NAS **(Supplemental Figure**

194   **4D)**. $V_{Ra\beta OHB}$ did not correlate with liver PDFF (r = 0.38, p value = 0.143), but trended towards a

195   positive correlation with AIRg (r = 0.46, p value = 0.081) **(Supplemental Figure 5A-B).** $V_{Ra\beta OHB}$

196   also positively correlated with circulating transaminase levels [AST, r = 0.51, P value = 0.041;

197   ALT, r = 0.52, P value = 0.037] **(Supplemental Figure 5C).** Despite the observed correlations

198   with ketogenesis, similar correlations were not observed for circulating non-esterified fatty acids

199   (NEFAs), a primary substrate for ketogenesis. Circulating NEFAs did not correlate with

200   ketogenesis ($V_{Ra\beta OHB}$) or with total plasma ketone bodies **(Figure 3D-E)**, suggesting variations in

201   ketogenesis were not driven by variations in the availability of NEFAs in these participants under

202   these conditions. Circulating NEFAs also did not correlate with NAS score (r = 0.15, P = 0.572,

203   **Figure 3F**). Moreover, NEFAs also did not correlate with whole body fat mass or percent

204   android fat, but did correlate with percent gynoid fat (r = 0.50, P value = 0.050) and inversely

205   correlated with the android/gynoid ratio (r = -0.55, P value = 0.028) **(Supplementary Figure**

206   **5D)**.

207   Though not included in NAS, fibrosis is also a strong indicator of MASLD progression.

208   Total fat oxidation trended towards a correlation with fibrosis (r = 0.49, P value = 0.056), and RE

209   production was significantly correlated with fibrosis (r = 0.50, P value = 0.047) **(Supplemental**

210   **Figure 6A-B).** Fibrosis was inversely correlated with the rate of anaplerosis relative to the TCA

211   cycle (V_{PEPCK} / V_{CS}) (r = -0.63, P value = 0.009), and positively correlated with the rate of the

212   TCA cycle relative to EGP (V_{CS} / V_{EGP}) (r = 0.52, P value = 0.038) **(Supplemental Figure 6C-D).**

213   These ratios provide insight into the distribution of REs harvested from fat oxidation, and

214   suggest that with MASLD progression, the sourcing of REs to glucose production may wane.

215   While these fluxes are modeled in participants at a single time point, and thus do not

216   demonstrate longitudinal relationships, these data demonstrate that ketogenesis and total fat

217   oxidation increase in proportion to liver injury, while TCA cycle flux remains relatively stable.

218   These results suggest that ketogenesis and fat oxidation could accelerate during the natural

219   history of MASLD progression to MASH. Given (i) this relationship between ketogenesis and

220   MASLD and (ii) the fact that ketogenesis is a strong predictor of total fat oxidation in the liver,

221   we sought to determine the mechanistic connections among these indices using mouse models.

222   ***Loss of HMGCS2 predisposes the liver to steatosis and dysregulated hepatic energy***

223   ***metabolism.*** Our previous findings in ex vivo perfused livers suggested that GNG was impaired

224   in the setting of ketogenic insufficiency (46, 52). Because hepatic GNG is bioenergetically

225   coupled to fat oxidation, this suggested that fat oxidation might be impaired in the absence of

226   ketogenesis. Nonetheless, ketogenesis insufficient mice maintained euglycemia when fasted,

227   due to compensation from hepatic glycogenolysis, and/or extrahepatic gluconeogenesis (46, 52,

228   54). To test if fat oxidation was impaired by ketogenic insufficiency in vivo, we fed littermate

229   control wild-type (WT) and hepatocyte-specific HMGCS2-null (HMGCS2-Liver-KO) mice a high-

230   fat, carbohydrate-restricted (HFCR) diet, and hypothesized that in the absence of dietary

231   carbohydrates, hepatic GNG would fail to support glycemia **(Figure 4A)**. We confirmed loss of

232   HMGCS2 function (48, 55) by demonstrating that chow-fed HMGCS2-Liver-KO mice failed to

233   mount a ketogenic response to fasting, but maintained a normal ratio of βOHB:AcAc **(Figure**

234   **4B-D)** (56)**.** When littermate control WT mice were placed on HFCR diet for 1 week, 4h fasted

235   total ketone bodies were elevated 3.3 ± 0.2-fold, as expected (Student's t-test, P value < 0.001);

236   however, only βOHB was increased, and not circulating AcAc **(Supplemental Figure 7A).** As a

237   result, the ratio of βOHB:AcAc was increased 10.7 ± 0.2-fold **(Supplemental Figure 7B).**

238   Unexpectedly, while circulating total ketones in HFCR diet-fed HMGCS2-Liver-KO mice ($662 \pm$

239   152 µM) trended lower than controls (1071 ± 349 µM) (Student's t-test, P value = 0.08), they

240   were markedly elevated compared to chow-fed HMGCS2-Liver-KO mice (66 ± 5 µM) **(Figure**

241   **4C, 4E).** Compared to littermate controls maintained on HFCR diet, HMGCS2-Liver-KO mice

242   markedly decreased the ratio of βOHB:AcAc, but increased the total amount of circulating L-

243   βOHB by 3.8 ± 0.1-fold, which does not contribute to mitochondrial $NADH:NAD^+$ ratio **(Figure**

244   **4F, Supplemental 7C-D).** To address whether the ketonemia in HFCR diet-fed HMGCS2-Liver-

245   KO mice was attributable to ketogenesis or to impairments in peripheral ketone body disposal,

246   we quantified static abundance of ketone bodies in liver tissue and found that HFCR diet-fed

247   HMGCS2-Liver-KO livers showed a $69 \pm 14\%$ diminution in total ketones (Student's t-test, P

248   value < 0.01), and increased liver L-βOHB, which together support impairment of ketogenesis in

249   livers of HFCR diet-fed HMGCS2-Liver-KO mice **(Supplemental Figure 7E-F).**

250   To determine the physiological response to HFCR diet in HMGCS2-Liver-KO mice, we

251   quantified gravimetric indices and metabolite concentrations after one week after transitioning

252   from chow. HMGCS2-Liver-KO mice lost more weight than littermate controls when fed the

253   HFCR diet but developed severe hepatomegaly **(Figure 5A-C).** This was accompanied by a 3.5

254   ± 0.1-fold accumulation of liver TAGs (**Figure 5D-E),** which could be reversed by refeeding mice

255   chow diet for one week **(Figure 5F).** In both the random-fed, and 4h fasted state, HMGCS2-

256   Liver-KO HFCR diet-fed mice had elevated plasma NEFAs, no difference in circulating TAGs,

257   decreased blood glucose, and depleted hepatic glycogen **(Figure 6A-H).**

258   To test the hypothesis that impaired hepatic fat oxidation could be linked to diminished

259   glycemia in HFCR diet-fed HMGCS2-Liver-KO mice, we quantified hepatic glucose and

260   associated oxidative fluxes in vivo in conscious, unrestrained mice, using a previously

261   established GC-MS-based approach (57–59). To accomplish this, vascular catheters were

262   placed in the carotid artery and jugular vein of mice fed chow diet. Five days post-surgery mice

263   were switched to HFCR diet for 2 days. Seven days post-surgery, ^2H_2O, [U-$^{13}C_3$]propionate, and

264   [6,6-$^2H_2$]glucose stable isotope tracers were infused, allowing quantification of in vivo fluxes via

265    $^2H/^{13}C$ metabolic flux analysis **(Figure 7A)** (51, 58, 59)**.** When fasted, HFCR diet-fed HMGCS2-

266   Liver-KO mice had lower rates of whole-body glucose production (V_{EGP}) [59.6 ± 8.2 µmol/min/kg

267   body weight (BW)], compared to littermate controls [90.1 ± 12 µmol/min/kg BW, Student's t-test,

268   P value = 0.003] (**Figure 7B**)**.** Body weight was not different between groups (data not shown).

269   Both littermate control WT and HMGCS2-Liver-KO mice showed very low rates of

270   glycogenolysis (V_{PYGL}), however, as expected, HFCR diet-fed HMGCS2-Liver-KO mice showed

271   a 31 ± 8% (Student's t-test, P value < 0.01) diminution in total GNG (V_{Aldo}), which was linked to

272   diminished sourcing of glucose from both glycerol (V_{GK}) and PEP (V_{Enol}) **(Figure 7C).** GNG

273   fluxes are tightly coupled to the entry (anaplerosis) and exit (cataplerosis) of nutrients through

274   the TCA cycle, thus we next examined glucose-linked hepatic oxidative fluxes. While

275   anaplerosis from propionyl-CoA (V_{PCC}) was decreased in HMGCS2-Liver-KO mice, most

276   anaplerotic fluxes were not different between genotypes (V_{PC}, V_{LDH}, and V_{PK+ME}). Cataplerosis

277   (V_{PCK}) was also similar between HMGCS2-Liver-KO and littermate controls (Student's t-test, P

278   value > 0.05) **(Figure 7D)**. However, HMGCS2-Liver-KO mice showed increased TCA cycle

279   fluxes as evidenced by higher V_{CS} (+72 ± 6%, Student's t-test, P value < 0.001) and V_{SDH} (+42 ±

280   6%, Student's t-test, P value < 0.01) **(Figure 7D).** Thus, the V_{PCK}/V_{CS} ratio was decreased 50 ±

281   10% (Student's t-test, P value < 0.001) in HMGCS2-Liver-KO mice, and V_{CS}/V_{EGP} ratio was

282   increased 158 ± 8% (Student's t-test, P value < 0.001) **(Supplemental Figure 8A).** Moreover,

283   while V_{PC} was unchanged, static concentrations of acetyl-CoA were increased 77 ± 17%

284   (Student's t-test, P value < 0.01) in livers of HFCR diet-fed HMGCS2-Liver-KO mice, indicating

285   an absence of allosteric activation of PC by acetyl-CoA **(Supplemental Figure 8B)**. Moreover,

286   succinyl-CoA and propionyl-CoA were decreased, also suggestive of diminished relative

287   anaplerosis **(Supplemental Figure 8B).** The total pools of energy adenylates (ATP, ADP, and

288   AMP) were diminished 39 ± 14% in livers of HFCR diet-fed HMGCS2-Liver-KO mice, with no

289   impairment in energy charge **(Supplemental Figure 8C-E)**. Static liver concentrations of redox

290   metabolites NAD^+ and NADH were also both diminished 45 ± 13% and 38 ± 14%, respectively,

291   but no difference in liver NAD^+/NADH ratio was observed in HFCR-fed HMGCS2-Liver-KO mice

292   **(Supplemental Figure 8F-H).** Together, these findings underscore interconnections among

293   ketogenesis, fat oxidation, anaplerosis/cataplerosis, and EGP. Relative responses of modeled

294   fluxes in HFCR diet-fed HMGCS2-Liver-KO mice quantified in vivo via intravenous infusions are

295   consistent with our prior observations using ex vivo portal vein liver perfusions in chow-fed

296   HMGCS2 knockdown mice, which revealed: (i) increased mitochondrial acetyl-CoA, (ii) elevated

297   V_{CS}, and (iii) diminished V_{PEPCK}/V_{CS} ratio (46, 52). We next sought to quantify the contribution of

298   ketogenesis to hepatic fat oxidation, and how this influences the course of MASLD-MASH.

299   ***Ketogenic insufficiency impairs total hepatic fat oxidation.*** To determine if ketogenic

300   insufficiency impaired hepatic fat oxidation **(Figure 8A)**, including those components accounted

301   for by ketogenesis and V_{CS}, we returned to ketogenesis insufficient ex vivo perfused livers in

302   carbohydrate-replete settings. Our group previously characterized the HMGCS2 antisense

303   oligonucleotide (ASO) knockdown liver and showed (i) abrogation of liver HMGCS2 protein, but

304   its preservation in non-hepatic tissues; (ii) abrogation of fasting-induced ketogenesis; (iii)

305   elevation of V_{CS} and V_{CS}/V_{GNG} ratio; and (iv) increased predisposition to steatotic liver injury (46,

306   47, 52, 56). Compared to control mice receiving scrambled ASO, the livers of chow-fed

307   ketogenesis insufficient mice exhibited an 80 ± 24% diminution in total fat oxidation (Student's t-

308   test, P value < 0.001), a 76 ± 24% impairment in REs generated from β-oxidation, and a strong

309   trend towards a decrease in total RE production rate (39 ± 23% Student's t-test, P value =

310   0.056), despite a trend toward a 70 ± 23% increase in TCA cycle-sourced REs (Student's t-test,

311   P value = 0.1108) **(Figure 8B-C).** There were no differences in REs generated through GNG.

312   Concordantly, in livers of HMGCS2 knockdown mice fed a sucrose-enriched, 42% kcal from fat

313   Western diet (WD) for 8 weeks, we observed V_{CS} was increased 155 ± 30% (Student's t-test, P

314   value = 0.03), and as such REs produced by the TCA cycle strongly trended towards a >2-fold

315   increase (Student's t-test, P value = 0.05), suggesting that loss of ketogenesis stimulates

316   terminal fat oxidation in the TCA cycle in WD-fed mice **(Figure 8D-F).** Nonetheless, the data

317   support the hypothesis that the rate of total fat oxidation is impaired by ketogenic insufficiency.

318   To address underlying mechanisms for impaired fat oxidation, we isolated mitochondria

319   from control C57BL/6NJ mouse livers and performed mitochondrial stress testing using our

320   standard creatine kinase (CK) clamp protocol, allowing quantification of respiratory flux (JO$_2$)

321   across variations in energy demand (ΔG$_{ATP}$) **(Figure 9A)** (60). Treatment of mitochondria with

322   hymeglusin (HG), a small molecule inhibitor of both HMGCS isoforms (HMGCS1 is cytoplasmic

323   enzyme and is thus not included in our mitochondrial preparations) showed the expected

324 diminution in HMG-CoA, as well as AcAc and βOHB within mitochondria, coinciding with

325 abrogated βOHB production rates in mitochondria stimulated with palmitoyl-L-carnitine + α-

326 ketoglutarate **(Figure 9B-C)** (61, 62). With increasing energy demand, JO_2 rates increased with

327 a diminished slope in HG-treated mitochondria, indicating an overall respiratory impairment due

328 to ketogenic insufficiency **(Figure 9D)**. This coincided with an accumulation of C2-C8 acyl-CoA

329 species, and a depletion in free CoA **(Figure 9E-F)**. Finally, mitochondrial redox was more

330 reduced [NAD(P)H, % reduced] in HG-treated mitochondria **(Figure 9G).** While this result may

331 appear to contradict the normal redox ratio observed in livers of HFCR-fed HMGCS2-Liver-KO

332 mice **(Supplemental Figure 8H)**, static concentrations of total redox nucleotides may not reflect

333 variations in cycling enzymatically-bound pools (53, 63). Taken together, these findings show

334 that ketogenic insufficiency impairs total hepatic fat oxidation in vivo, ex vivo, and in isolated

335 mitochondria. A potential contributor to this impairment includes free CoA trapping, which

336 impedes procession though β-oxidation and the TCA cycle, which is supported by our prior

337 findings (46). A second contributor to diminished fat oxidation rates is reduced mitochondrial

338 matrix redox potential in the setting of ketogenic insufficiency, captured in this flux-based assay

339 that quantifies redox nucleotide turnover among actively cycling enzymatic pools.

340 ***Loss of mitochondrial βOHB dehydrogenase (BDH1) impairs hepatic fat oxidation but***

341 ***does not provoke liver injury.*** Ketogenic insufficiency via loss of HMGCS2 function causes

342 steatotic liver injury (45–49). Our findings show that loss of HMGCS2 diminishes rates of liver

343 fat oxidation in a manner correlated with more reduced mitochondrial redox potential. To

344 interrogate the role of the ketogenic reaction directly regulating mitochondrial redox potential,

345 catalyzed by mitochondrial BDH1 (which converts AcAc and NADH to βOHB and NAD$^+$) in (i)

346 total hepatic fat oxidation and (ii) the response to steatotic liver injury, we studied mice in which

347 BDH1 had been deleted specifically in hepatocytes (BDH1-Liver-KO mice) **(Figure 10A)**. Our

348 prior studies demonstrated impairments of oxidative metabolism in BDH1-Liver-KO mice on

349   chow diet (53). Here, we fed mice 42% kcal fat WD for 16 weeks. As expected, circulating

350   βOHB and total ketones were diminished after an 18h fast **(Supplemental Figure 9A)**. Body

351   weights, liver weights, and blood glucose were unchanged **(Supplemental Figure 9B-D).** Livers

352   were then perfused ex vivo with a physiologically relevant mixture of long-chain fatty acids

353   (LCFAs) conjugated to bovine serum albumin (BSA). While there was no significant diminution

354   in total ketogenesis in livers of BDH1-Liver-KO mice, all ketone bodies emerged as AcAc, with

355   no hepatic βOHB production **(Figure 10B-C).** V_{EGP} was diminished 26 ± 13% (Student's t-test, P

356   value = 0.0390) in livers of BDH1-Liver-KO mice, which coincided with a 48 ± 12% and 30 ±

357   13% decrease in sourcing of glucose from both PEP (Student's t-test, P value < 0.001) and

358   glycogen (Student's t-test, P value = 0.04), respectively **(Supplemental Figure 9E-G).**

359   Consistent with our previous findings observed in chow-fed mice, the rates of pyruvate cycling

360   (V_{PK+ME}), anaplerosis and cataplerosis (V_{PEPCK}), and TCA cycle turnover (V_{CS}) were all

361   suppressed 42 ± 16% (Student's t-test, P value = 0.0043), 15 ± 13% (Student's t-test, P value =

362   0.0005), and 39 ± 17% (Student's t-test, P value = 0.0160), respectively, in livers of BDH1-Liver-

363   KO mice on WD **(Figure 10D).** Furthermore, total fat oxidation was decreased 26 ± 12%

364   (Student's t-test, P value = 0.0170) and RE production rate was decreased 20 ± 10% (Student's

365   t-test, P value = 0.0259) **(Figure 10E-F),** demonstrating that loss of the NAD^+ regenerating step

366   of ketogenesis alone is sufficient to impair overall fat oxidation in the liver.

367   To determine whether the diminution in hepatic fatty acid (FA) oxidation in livers of

368   BDH1-Liver-KO mice was linked to increased steatosis or injury in mice fed a 42% kcal fat WD

369   for 16 weeks, we performed histological and molecular analyses. H&E staining showed normal

370   lipid droplet storage, and no evidence of increased fibrosis via picrosirius red staining compared

371   to controls **(Figure 10G).** Gene expression biomarkers of fibrosis (*Col1a1, Col3a1, Col4a1,*

372   *Acta2*) were unchanged and quantities of tissue lipid peroxides were not increased in livers of

373   BDH1-Liver-KO mice **(Figure 10H-I).** Maintenance of independent cohorts of BDH1-Liver-KO

374   and littermate control mice on a 60% kcal high fat diet (HFD) for 16 weeks also showed no

375   evidence of increased steatosis, inflammation, or fibrosis – with a trend towards a diminution in

376   fibrosis in livers of BDH1-Liver-KO mice (56 ± 30%, Student's t-test, P value = 0.06)

377   **(Supplemental Figure 10A-C)**. Moreover, gene expression biomarkers of fibrosis and

378   inflammation were diminished in livers of BDH1-Liver-KO mice fed a 60% HFD **(Supplemental**

379   **Figure 10C).** Lastly, we induced liver injury in mice by feeding a fibrogenic choline-deficient,

380   methionine-limited high fat (62% kcal) diet for 16 weeks, but did not detect worsened steatosis,

381   injury, fibrosis, or inflammation in BDH1-Liver KO mice **(Supplemental Figure 10D-E).**

382   Collectively, these findings demonstrate (i) that ketogenesis is required to maintain hepatic fat

383   oxidation and its coupling to V_{EGP}, with loss of either HMGCS2 or BDH1 impairing hepatic fat

384   oxidation, and (ii) that the impairment in fat oxidation does not fully explain why loss of

385   HMGCS2 predisposes the liver to HFD-induced liver injury.

386

387

388

389

390

391

392

393

394

395

396   **Discussion**

397   The natural history of MASLD-MASH proceeds through derangements of both liver-autonomous

398   and systemic metabolic pathways, among many cell types. Characteristic metabolic signatures

399   include imbalanced lipid synthesis (DNL and TAG synthesis) and disposal (mitochondrial fat

400   oxidation and TAG secretion as VLDL). While most studies concur that DNL is augmented, and

401   VLDL secretion does not match the rate of lipid accumulation, controversy surrounds variations

402   in the rate of mitochondrial fat oxidation and whether variations in this rate have a causal role.

403   This impacts the selection of therapeutic molecular targets worthy of pursuit. In this study, we

404   quantified hepatic oxidative fluxes in humans with histologically confirmed MASLD-MASH and

405   demonstrated that the histopathological degree of liver injury was positively correlated with

406   ketogenesis and total fat oxidation but not TCA cycle turnover. Use of mouse models suggested

407   a driver role of ketogenesis in overall hepatic fat oxidation and a causal role in preventing liver

408   injury, as elimination of HMGCS2 diminished hepatic fat oxidation. This decrement correlates

409   with increased steatotic liver injury, as shown in other studies in the setting of ketogenic

410   insufficiency (45–49). Thus, the increased ketogenesis observed in patients with higher NAS

411   may serve a compensatory mechanism, increasing fat disposal through oxidation, in the

412   absence of increases in the rates of TCA cycle-linked terminal oxidation. This position is

413   challenged, however, by the results observed in mice lacking hepatocyte-BDH1, whose

414   deficiency also diminishes hepatic fat oxidation rates, but is not associated with worsened

415   steatotic liver disease. In fact, signatures of a modestly adaptive response to diminished hepatic

416   fat oxidation are evident in the livers of BDH1-Liver-KO mice. Taken together, these results

417   suggest that while ketogenic sufficiency may be important to slow the progression of MASLD,

418   the salutary mechanism conferred by ketogenesis may not only relate to maximizing hepatic fat

419   oxidation. Therefore, approaches aimed primarily at stimulating hepatic fat oxidation may not

420   ameliorate the course of commonly-observed MASLD, and could exacerbate liver injury.

421   Quantified rates of hepatic fat oxidation in humans with MASLD, relative to steatosis-

422   free, but weight-matched controls, have reported disparate observations (22–25, 30–37, 50, 64,

423   65). Much of this may relate to the populations studied, including (i) the stage of progression; (ii)

424   the degree of adiposity and insulin resistance; (iii) whether or not the participant was weight-

425   neutral; (iv) the genotype (e.g., *PNPLA3*); (v) whether the participant was fed, fasting, or

426   undergoing a clamp study; and lastly, (vi) the specific methodology employed. While in vivo

427   hepatic oxidative fluxes have been quantified in humans with uncomplicated MASLD, and

428   isolated mitochondrial function has been measured in liver biospecimens harvested from

429   participants with MASH, in vivo hepatic oxidative fluxes have not been previously quantified in

430   humans with histologically-confirmed MASH. In well-performed studies by the Burgess and

431   Browning group, ketogenesis negatively correlated with worsening hepatic steatosis in fasting

432   overweight and obese participants with BMI ≤ 35 (22, 37). Moreover, circulating ketones and

433   expression levels of ketogenic enzymatic machinery decreased within worsening NAS in a

434   bariatric surgery cohort studied by the Rector group, but no study has tested whether

435   endogenous ketogenesis correlates with histopathologically-confirmed liver injury (33, 34).

436   Consistent with our findings, a recent study in non-obese participants with MASLD by the

437   Petersen and Shulman group showed that participants with compounding cardiometabolic

438   disturbances have increased rates of βOHB turnover in comparison to participants with simple

439   steatosis alone, or with healthy livers, but liver biopsies were not available in that study (27).

440   The cohort studied in our experiments reflects a population with advanced obesity at elevated

441   risk of progression from MASH to cirrhosis, and among the metabolic fluxes modeled, the only

442   direct correlate of NAS was endogenous ketogenesis. We propose that the escalation of TCA

443   cycle flux early in the progression of MASLD may become attenuated with further progression,

444   and indeed, the two participants we studied with the greatest V_{CS} (>12 μmol/min/kg-LBM) had

445   NAS 4, and those exhibiting a NAS > 4 did not exceed 10 μmol/min/kg-LBM. Thus with respect

446   to variations of TCA cycle flux, our data are generally consistent with those of the Burgess and

447   Browning group (22, 25). Moreover, while impaired fasting ketogenesis was reported in a

448   relatively leaner population of participants than those studied here, the same subjects showed

449   elevated ketosis in the postabsorptive state and during a clamp (22). Taken together, the

450   aggregate data in both humans and mouse models suggest that ketogenesis may serve an

451   adaptive counterregulatory role, especially with further MASH progression.

452   Our findings in mouse models of altered ketogenesis suggest that impairments in

453   hepatic fat oxidation in ketogenic insufficiency does not relate in a direct manner to liver injury,

454   implying that the link between ketogenesis and MASLD-MASH progression involves attributes of

455   ketogenesis beyond its contribution to hepatic fat oxidation. Concordance between our

456   observations in modeled hepatic fluxes of the human participants with MASH and mouse

457   models of ketogenic insufficiency strongly substantiate this claim. In addition to the direct

458   association between ketogenesis and human NAS score, increasing histopathological evidence

459   of fibrosis was inversely correlated with V_{PEPCK}/V_{CS} ratio and directly with V_{CS}/V_{EGP} ratio

460   **(Supplemental Figure 6C-D),** suggestive of decoupling between TCA cycle flux and sourcing

461   of its derived REs to GNG with increasing liver injury. Similarly, V_{PCK}/V_{CS} ratio was decreased in

462   steatosis and injury-prone HMGCS2-Liver-KO mice, and V_{CS}/V_{EGP} ratio was increased

463   **(Supplemental Figure 8A)**. Conversely, this imbalance was not observed in livers of BDH1-

464   Liver-KO mice, whose V_{PEPCK}, V_{EGP}, and V_{CS} were all coordinately diminished **(Figure 10D).**

465   Alternatively, and not mutually exclusively, mechanisms linked to the increase in AcAc

466   production in livers of BDH1-Liver-KO mice could explain why the loss of BDH1 protects the

467   liver from injury (47).

468   Recently, we reported a role for ketogenesis in supporting FA elongation and PUFA

469   homeostasis in the liver (48). We demonstrated (i) ketogenesis furnishes hepatocytes with

470   malonyl-CoA for FA biosynthesis, via both DNL and FA elongation, and (ii) incorporation of

471   ketone body-derived carbon into FA elongation requires the cytosolic enzyme acetoacetyl-CoA

472 synthetase (AACS), through a metabolic pathway independent of ketone-sourced DNL.

473 Furthermore, we demonstrated that loss of HMGCS2 impairs FA elongation and diminishes

474 hepatic PUFAs, suggesting the ketogenesis could influence mitochondrial function and VLDL

475 secretion through PUFA-dependent mechanisms, though these possibilities have not yet been

476 tested. It is tempting to speculate that the pathway linking ketogenesis to PUFA biosynthesis

477 explains the protective nature of ketogenesis in MASLD-MASH progression, and the

478 observation that AcAc production is increased in the absence of BDH1 suggests that FA

479 elongation and PUFA biosynthesis could be stimulated in a substrate-driven manner. PUFAs

480 inhibit DNL in the liver via inhibiting SREBP1c mediated gene transcription (66–71), and

481 therefore the rise in ketone body-sourced PUFAs in the BDH1 KO could drive both acute and

482 chronic inhibition of DNL. This hypothesis is further supported by the observation that loss of

483 HMGCS2 induces a DNL gene expression profile (46, 48).

484   Collectively, these findings in humans with MASH and in ketogenesis insufficient mice

485 suggest that ketogenesis may compensate in a fat-overloaded, progressively injured liver,

486 thereby maintaining rates of fat oxidation, but perhaps just as importantly, by burning fat through

487 a metabolic pathway that confers additional benefits that terminal oxidation in the TCA cycle

488 may not bestow. The specific regulatory mechanisms that coordinate the fate of β-oxidation-

489 derived acetyl-CoA through the TCA cycle or ketogenesis, remain incompletely understood.

490 Classical mechanisms include oxaloacetate availability, allosteric regulation of citrate synthase,

491 NADH redox potential, and ΔG_{ATP}. Physiological variation in the abundance of HMGCS2 protein

492 could serve as a regulatory mechanism, but this has not been definitively proven. Our

493 observation that ketogenesis did not correlate with circulating NEFAs supports the notion that

494 liver-autonomous mechanisms mediate the acceleration in ketogenesis in the setting of

495 worsened liver injury. Irrespective, the pathways through which ketogenesis and ketone bodies

496 could influence DNL, PUFA synthesis, VLDL secretion, fat oxidation, and canonical signaling

497   pathways, opens opportunities to understand the range of therapeutic opportunities for ketone

498   bodies to ameliorate MASLD.

499   **Limitations.** The human studies are limited by a small sample size (16 participants), and were

500   predominately female (15 female, 1 male). While all participants were insulin resistant, only one

501   participant had diabetes, so it is not possible to make conclusions relevant in the scope of

502   MASLD within diabetes. Two independent experimental approaches were leveraged to delete

503   HMGCS2 protein in mice, but the concordance in phenotypes across these models supports the

504   rigor of our findings. Using metabolic flux modeling, we demonstrated that disruption of

505   ketogenesis impaired overall hepatic fat oxidation, which was quantified via an indirect flux

506   modeling-based assay predicated on the assumption that mitochondrial acetyl-CoA turnover at

507   steady-state is mathematically equivalent to 2 x total ketogenesis (V_{RaTKB}) + TCA cycle turnover

508   (V_{CS}) + acetogenesis ($V_{Acetate}$). A limitation of this approach is the assumption that fat oxidation is

509   primarily sourced from exogenous fat during perfusions, and the assumption that octanoate

510   sources little acetate. The findings, however, are reinforced by the concordance among all the

511   fluxes modeled across all orthogonal methodologies employed. Collectively, an impairment in

512   fat oxidation was consistently observed in the setting of ketogenic insufficiency, as shown

513   across various models including: (i) in vivo HFCR-diet-fed HMGCS2-Liver-KO mice; (ii) ex vivo

514   perfused livers from HMGCS2 ASO-knockdown mice maintained on either chow or WD; (iii) ex

515   vivo perfused livers from BDH1-Liver-KO mice maintained on chow or WD; and (iv) isolated

516   mitochondria treated with HG. Collectively, these data strongly support the hypothesis that

517   ketogenesis plays an integral role in regulating fat oxidation. A modest limitation of in vivo

518   ketogenesis measurements in humans was that ketogenesis was modeled as a single pool, with

519   V_{RaAcAc} calculated from $V_{Ra\beta OHB}$ and the ratio of βOHB:AcAc. Future experiments will infuse

520   independent [^{13}C]AcAc and [^{13}C]βOHB tracers to directly measure V_{RaAcAc}, and interconversion

521   of AcAc and βOHB through BDH1 via a two-pool model.

522 **Materials and Methods**

523 See supplemental methods for detailed methodology and calculations.

524 *Sex as a biological variable.* Males and females were studied, as delineated in the figure

525 legends. However, sex as a biological variable was not addressed.

526 *Human MASLD-MASH study design.* Sixteen participants with BMI ≥ 35 and liver PDFF > 5%

527 were recruited. Insulin sensitivity and body composition were assessed via FSIVGTT and DXA

528 imaging, respectively, followed by in vivo hepatic oxidative flux measurements. Prior to flux

529 measurements, a liver biopsy was obtained for determination of the NAFLD activity score

530 (NAS).

531 *Stable isotope delivery in humans.* Fasted participants were provided with three equal doses of

532 70% deuterated water (^2H_2O, 5 g/kg body water), along with 0.5% ^2H_2O available for ad libitum

533 consumption to enrich body water, and two doses of oral [U-$^{13}C_3$]propionate (300 mg/dose) to

534 label TCA cycle intermediates for profiling of hepatic mitochondrial fluxes. Intravenous stable

535 isotope infusion began with [3,4-$^{13}C_2$]glucose [0.563 mg/kg BW bolus, immediately followed by a

536 two-hour infusion (0.00563 mg/min/kg BW)], and D-[U-$^{13}C_4$]βOHB [1 mg/kg BW bolus,

537 immediately followed by two-hour infusion (0.01 mg/min/kg BW)]. At the end of the 2h infusion,

538 ~50 mL of blood was drawn, centrifuged to isolate plasma, then aliquots were frozen at -80ºC

539 until further analysis.

540 *$^2H/^{13}C$ NMR hepatic flux modeling.* The positional ^{13}C and ^2H isotopomers of plasma glucose

541 encodes quantitative information about hepatic biochemical pathways, thus allowing for

542 noninvasive modeling of hepatic metabolism in vivo. Direct quantification of the positional

543 isotopomer populations of plasma glucose was achieved using ^{13}C and ^2H NMR, post

544 derivatization into 1,2-isopropylidene glucofuranose (monoacetone glucose [MAG]) as

545 previously described (25, 36, 51, 52).

546   *Quantifying whole-body βOHB turnover.* βOHB turnover was calculated at metabolic and

547   isotopic steady-state from the dilution of intravenously infused D-[U-$^{13}C_4$]βOHB using the

548   equation:

549   Whole Body βOHB Turnover (µmol βOHB/min/kg BW)= $\frac{F}{(\frac{TTR}{TTR+1})}$ - F

550   [^{12}C]βOHB and [U-$^{13}C_4$]βOHB were quantified using UHPLC-MS/MS, then the Tracer:Tracee

551   ratio (TTR, [U-$^{13}C_4$]βOHB / [^{12}C]βOHB) in plasma and the tracer infusion rate (F) was used to

552   calculate whole-body βOHB turnover rates. Because the liver is the primarily site of systemic

553   ketone body production, whole-body βOHB turnover at steady-state is mathematically

554   equivalent to hepatic endogenous βOHB production rates **($V_{RaβOHB}$).** After flux measurements,

555   turnover rates are corrected for LBM from DXA imaging, and expressed as µmol βOHB turned

556   over/min/kg-LBM.

557   *Quantifying whole-body glucose turnover.* Glucose turnover was calculated at metabolic and

558   isotopic-steady state from the dilution of intravenously infused [3,4-$^{13}C_2$]glucose using the

559   equation:

560   Whole Body Glucose Turnover (mg glucose/min/kg BW) $= F \ x \ (\frac{Li-Lp}{Lp})$

561   where F is tracer infusion rate, L_p is fractional ^{13}C enrichment of the plasma glucose pool

562   measured via ^{13}C NMR, and L_i is the enrichment of infused glucose, assumed to be 99%. In the

563   fasted state the majority (>90%) of whole-body glucose production is derived from the liver,

564   therefore total glucose turnover rates are mathematically equivalent to total hepatic EGP rates

565   **(V_{EGP}).** Using the DXA scan information, final flux units were expressed as µmoles glucose

566   turned over/min/kg-LBM.

567   *Quantifying hepatic glucose sourcing fluxes.* Using the ^2H enrichment patterns encoded in

568   plasma glucose, the fractional contribution of various glucose sourcing pathways was

569   determined, then multiplied by total EGP **(V_{EGP})** to calculate absolute flux through each hepatic

570   glucose sourcing pathway using the following equations:

571   Glycogenolysis **($V_{Glycogen}$)** (μmol glucose/min kg LBM) = V_{EGP} x $(\frac{H2-H5}{H2})$

572   Gluconeogenesis from Glycerol **($V_{Glycerol}$)** (μmol glucose/min/kg LBM) = V_{EGP} x $\left(\frac{H5-H6s}{H2}\right)$

573   Gluconeogenesis from PEP **(V_{PEP})** (μmol glucose/min/kg LBM) = V_{EGP} x $(\frac{H6s}{H2})$

574   where H2, H5 and H6s correspond to the relative ^{2}H enrichment at the 2, 5 and 6s carbons of

575   MAG.

576   *Quantifying hepatic oxidative fluxes.* The rate of hepatic TCA cycle turnover, anaplerosis,

577   cataplerosis and pyruvate cycling can be modeled in the liver using the ^{13}C isotopomers that

578   arise at C2 of plasma glucose from orally administered [U-^{13}C$_3$]propionate using the following

579   equations:

580   Pyruvate Cycling **(V_{PK+ME})** (μmol/min/kg LBM) = 2 x V_{PEP} x $\left(\frac{D12-Q}{Q-D23}\right)$

581   Anaplerosis **(V_{PC})** and Cataplerosis **(V_{PEPCK})** (μmol/min/kg LBM) = 2 x V_{PEP} x $\left(\frac{D12-D23}{Q-D23}\right)$

582   TCA Cycle Turnover **(V_{CS})** (μmol/mi /kg LBM) = 2 x V_{PEP} x $\left(\frac{D23}{Q-D23}\right)$

583   where D12 represents the doublet arising when C1 and C2 of glucose are labeled, D23

584   represents the doublet arising when C2 and C3 are labeled, and Q is the quartet arising when

585   C1, C2 and C3 are all labeled.

586   *Quantifying hepatic fat oxidation rates.* In the fasted liver, β-oxidation derived acetyl-CoA is (i)

587   principally converted to ketone bodies which are largely released from the liver, (ii) terminally

588   oxidized in the TCA cycle, or (iii) secreted as acetate. By assuming that the liver is in a

589   metabolic steady-state, the rate of acetyl-CoA production via β-oxidation can be assumed to be

590   equal to the rate of acetyl-CoA disposal, thereby allowing total fat oxidation rates to be indirectly

591   quantified as the sum of all disposal routes for hepatic acetyl-CoA as follows:

592   Total Fat Oxidation (µmol/min/kg LBM) = 2 x ($V_{Ra\beta OHB}$ + V_{RaAcAc}) + V_{CS} + $V_{Acetate}$

593   Fat oxidation is expressed in µmoles of acetyl-CoA turned over/min/kg-LBM. $V_{Ra\beta OHB}$ was

594   measured via a tracer dilution of intravenously infused D-[U-^{13}C$_4$]βOHB as described above.

595   V_{RaAcAc} was calculated from $V_{Ra\beta OHB}$ turnover rates and the ratio of plasma βOHB:AcAc. V_{CS} was

596   measured as described above. Hepatic acetate production rate ($V_{Acetate}$) was assumed to be

597   negligible in humans.

598   *Quantifying hepatic RE production.* The production of RE's, principally NADH and FADH$_2$, can

599   be estimated from the stoichiometry of the above fluxes as previously described (35, 72) using

600   the equations:

601   **(RE$_{AcAc}$)** = 3.5 x V_{RaAcAc}

602   **(RE$_{\beta OHB}$)** = 2.5 x $V_{Ra\beta OHB}$

603   **(RE$_{\beta ox-CS}$)** = 1.75 x V_{CS}

604   **(RE$_{TCA-only}$)** = 4 x $V_{CS.}$

605   **(RE$_{GNG}$)** = $V_{Glycerol-Triose}$ − (0.1 x $V_{PEP-Triose}$)

606   Total REs generated from β-oxidation was estimated as the sum of REs accounted for by

607   ketogenesis [AcAc, RE$_{AcAc}$; and βOHB, RE$_{\beta OHB}$] and TCA cycle turnover (RE$_{\beta ox-CS}$) as follows:

608   REs generated from β-oxidation **(RE$_{\beta OX}$)** = RE$_{AcAc}$ + RE$_{\beta OHB}$ + RE$_{\beta ox-CS}$

609   Total RE turnover was calculated as the sum of REs from β-oxidation (RE$_{\beta OX}$), TCA cycle

610   dehydrogenases (RE$_{TCA-only}$), and the dehydrogenases of GNG (RE$_{GNG}$) using the equation:

611   Total RE production rate (µmol RE/min/kg-LBM) = RE$_{\beta OX}$ + RE$_{TCA-only}$ + RE$_{GNG}$

612   *Animal models and diets.* Hepatocyte-specific HMGCS2 null mice (HMGCS2-Liver-KO), BDH1

613   null (BDH1-Liver-KO), and *Hmgcs2* ASO-mediated null mice were generated as described

614   previously (46, 48, 53, 55, 73, 74). Food and water were provided ad libitum. Mice were fed

615   either a standard chow diet, 42% kcal from fat WD, 60% kcal from fat HFD, 62% kcal from fat

616   choline-deficient methionine-limited HFD, or 90.5% kcal from fat HFCR diet.

617   *Mouse liver health assessment.* Following euthanasia, mouse liver sections were frozen or fixed

618   in 10% neutral buffered formalin. Formalin-fixed tissue was used for histological analysis.

619   Frozen liver tissue was assayed for total TAGs, glycogen content, oxidized lipid species, and

620   abundance of mRNA markers.

621   *Serum NEFAs, TAGs, and blood glucose measurements.* Serum NEFAs (Wako, 633-52001)

622   and TAGs (Thermo, TR22421) were measured spectrophotometrically using commercially-

623   available assays. Blood glucose was measured using glucose meters (Metene).

624   *Quantification of glucose, ketone bodies, and acetate.* Ketone bodies (AcAc and βOHB) were

625   quantified using UHPLC-MS/MS as described previously (53, 56). Glucose, acetate, and βOHB

626   was quantified during perfusions via ^{1}H-NMR.

627   In vivo *^{2}H/^{13}C metabolic flux analysis in conscious unrestrained mice.* To measure hepatic

628   metabolic fluxes in conscious mice ^{2}H$_2$O, [6,6-^{2}H$_2$]glucose, and [U-^{13}C]propionate were

629   intravenously delivered into fasted mice, then GC-MS was employed to determine the isotopic

630   enrichment of three glucose fragments. Using a metabolic reaction network constructed using

631   Isotopomer Network Compartmental Analysis (INCA) software, which defines the carbon and

632   hydrogen atom transitions for hepatic glucose and associated oxidative reactions, the relative

633   reaction velocities (V) (i.e., flux) through each network reaction was determined relative to CS

634   flux (V_{CS}). The known [6,6-^{2}H$_2$]glucose infusion rate was then used to calculate absolute

635   reaction velocities.

636   *Quantifying energy charge, redox state and short-chain acyl-CoAs.* Energy nucleotides, redox

637   nucleotides, and high-energy thioester containing acyl-CoAs were measured via LC-MS/MS,

638   and energy charge and redox state were calculated.

639   *Flux calculations in perfused livers.* Stable-isotope based flux modeling used in vivo in humans

640   and rodents as described above was used to study metabolism of the ex vivo perfused liver as

641   described previously, with minor modifications (52).

642   *Hepatic fat oxidation and RE production calculations in perfused livers.* In perfusions, total fat

643   oxidation was calculated as:

644   Total Fat Oxidation (µmol/min/kg LBM) = 2 ($V_{Ra\beta OHB}$ + V_{RaAcAc}) + V_{CS} + $V_{Acetate}$

645   and expressed as µmol acetyl-CoA turned over/min/g liver. The same model, assumptions, and

646   equations used to model RE production rate in vivo in humans was used to model RE

647   production rate in ex vivo perfused livers, with minor modifications.

648   *Mitochondrial respiratory control.* Liver mitochondria were isolated and steady-state oxygen

649   consumption rates (JO_2) were determined using a modified version of the creatine kinase (CK)

650   energetic clamp as described previously (75). Mitochondrial NAD(P)H to NAD(P)+ ratio, acyl-

651   CoAs and organic acids, and βOHB production was assayed post CK-clamp.

652   *Statistics and data analysis.* All analyses were performed using GraphPad Prism version 9.

653   Unpaired 2-tailed Student's t-tests or 1-way ANOVA, was used to determine statistically

654   significant differences. P-value < 0.05 was accepted as significant for all tests. Information

655   about statistical analysis is included in each figure legend. Data are presented as mean ± SD,

656   unless otherwise indicated.

657   *Study approval.* The University of Minnesota's Institutional Review Board (IRB) approved the

658   human study protocol and methods. All human participants provided written informed consent.

659   All animal experiments were approved by the Institutional Animal Care and Use Committee

660   (IACUC) at the University of Minnesota.

661   *Data availability.* All data required for evaluation of conclusions are included in this manuscript.

662   Individual data points are plotted in each graph, or included in Supporting Data Values file.

663

664   **Author Contributions**

665   Research studies designed by EDQ, DBS, ABN, ABC, SBC, KF, DAD, JRR, ASW, DMM, SI,

666   CCH, PP and PAC. Data was acquired and analyzed by EDQ, DBS, ABN, ABC, SBC, KF, DAD,

667   JRR, PJB, AH, JRG, SJ, FIR, ASW, DMM, CCH and PP. SI and PAC also helped analyze data.

668   Writing of the initial manuscript draft was done by EDQ, PP and PAC. All authors edited the

669   manuscript. Funding was acquired by SI, CCH and PAC.

670

671   **Acknowledgements**

References

1. Younossi ZM, et al. The global epidemiology of nonalcoholic fatty liver disease (NAFLD) and nonalcoholic steatohepatitis (NASH): a systematic review. *Hepatology.* 2023;77(4):1335.

2. Riazi K, et al. The prevalence and incidence of NAFLD worldwide: a systematic review and meta-analysis. *Lancet Gastroenterol Hepatol.* 2022;7(9):851–861.

3. Ipsen DH, Lykkesfeldt J, Tveden-Nyborg P. Molecular mechanisms of hepatic lipid accumulation in non-alcoholic fatty liver disease. *Cell Mol Life Sci.* 2018;75(18):3313–3327.

4. Postic C, Girard J. Contribution of de novo fatty acid synthesis to hepatic steatosis and insulin resistance: lessons from genetically engineered mice. *J Clin Invest.* 2008;118(3):829–838.

5. Pierantonelli I, Svegliati-Baroni G. Nonalcoholic Fatty Liver Disease: Basic Pathogenetic Mechanisms in the Progression From NAFLD to NASH. *Transplantation.* 2019;103(1):e1.

6. Sheka AC, et al. Nonalcoholic Steatohepatitis: A Review. *JAMA.* 2020;323(12):1175–1183.

7. Harrison SA, et al. A Phase 3, Randomized, Controlled Trial of Resmetirom in NASH with Liver Fibrosis. *N Engl J Med.* 2024;390(6):497–509.

8. Ferguson D, Finck BN. Emerging therapeutic approaches for the treatment of NAFLD and type 2 diabetes mellitus. *Nat Rev Endocrinol.* 2021;17(8):484–495.

9. Jang H, et al. Outcomes of Various Classes of Oral Antidiabetic Drugs on Nonalcoholic Fatty Liver Disease. *JAMA Intern Med.* 2024;184(4):375–383.

10. Mak SK, et al. Intracardiac thrombus in an adult patient with nephrotic syndrome. *Nephrol Dial Transplant Off Publ Eur Dial Transpl Assoc - Eur Ren Assoc.* 1996;11(8):1627–1630.

11. Syed-Abdul MM, et al. Isotope Labeling and Biochemical Assessment of Liver-Triacylglycerol in Patients with Different Levels of Histologically-Graded Liver Disease. *J Nutr*. 2023;153(12):3418–3429.

12. Lambert JE, et al. Increased De Novo Lipogenesis Is a Distinct Characteristic of Individuals With Nonalcoholic Fatty Liver Disease. *Gastroenterology*. 2014;146(3):726–735.

13. Flannery C, et al. Skeletal muscle insulin resistance promotes increased hepatic de novo lipogenesis, hyperlipidemia, and hepatic steatosis in the elderly. *Diabetes*. 2012;61(11):2711–2717.

14. Donnelly KL, et al. Sources of fatty acids stored in liver and secreted via lipoproteins in patients with nonalcoholic fatty liver disease. *J Clin Invest*. 2005;115(5):1343–1351.

15. Schwarz J-M, et al. Hepatic de novo lipogenesis in normoinsulinemic and hyperinsulinemic subjects consuming high-fat, low-carbohydrate and low-fat, high-carbohydrate isoenergetic diets. *Am J Clin Nutr*. 2003;77(1):43–50.

16. Diraison F, Moulin P, Beylot M. Contribution of hepatic de novo lipogenesis and reesterification of plasma non esterified fatty acids to plasma triglyceride synthesis during non-alcoholic fatty liver disease. *Diabetes Metab*. 2003;29(5):478–485.

17. Araya J, et al. Increase in long-chain polyunsaturated fatty acid n - 6/n - 3 ratio in relation to hepatic steatosis in patients with non-alcoholic fatty liver disease. *Clin Sci Lond Engl 1979*. 2004;106(6):635–643.

18. Allard JP, et al. Nutritional assessment and hepatic fatty acid composition in non-alcoholic fatty liver disease (NAFLD): a cross-sectional study. *J Hepatol*. 2008;48(2):300–307.

19. Arendt BM, et al. Nonalcoholic fatty liver disease is associated with lower hepatic and erythrocyte ratios of phosphatidylcholine to phosphatidylethanolamine. *Appl Physiol Nutr Metab Physiol Appl Nutr Metab*. 2013;38(3):334–340.

20. Spooner MH, Jump DB. Nonalcoholic Fatty Liver Disease and Omega-3 Fatty Acids: Mechanisms and Clinical Use. *Annu Rev Nutr*. 2023;43(1):199–223.

21. Spooner MH, et al. Time course of western diet (WD) induced nonalcoholic steatohepatitis (NASH) in female and male Ldlr-/- mice. *PloS One*. 2023;18(10):e0292432.

22. Fletcher JA, et al. Impaired ketogenesis and increased acetyl-CoA oxidation promote hyperglycemia in human fatty liver. *JCI Insight*. 2019;4(11). https://doi.org/10.1172/jci.insight.127737.

23. Koliaki C, et al. Adaptation of Hepatic Mitochondrial Function in Humans with Non-Alcoholic Fatty Liver Is Lost in Steatohepatitis. *Cell Metab*. 2015;21(5):739–746.

24. Satapati S, et al. Elevated TCA cycle function in the pathology of diet-induced hepatic insulin resistance and fatty liver[S]. *J Lipid Res*. 2012;53(6):1080–1092.

25. Sunny NE, et al. Excessive Hepatic Mitochondrial TCA Cycle and Gluconeogenesis in Humans with Nonalcoholic Fatty Liver Disease. *Cell Metab*. 2011;14(6):804–810.

26. Petersen KF, et al. Assessment of Hepatic Mitochondrial Oxidation and Pyruvate Cycling in NAFLD by 13C Magnetic Resonance Spectroscopy. *Cell Metab*. 2016;24(1):167–171.

27. Petersen KF, et al. Glucagon promotes increased hepatic mitochondrial oxidation and pyruvate carboxylase flux in humans with fatty liver disease. *Cell Metab*. 2024;0(0). https://doi.org/10.1016/j.cmet.2024.07.023.

28. Lund MT, et al. Hepatic mitochondrial oxidative phosphorylation is normal in obese patients with and without type 2 diabetes. *J Physiol*. 2016;594(15):4351–4358.

29. Kotronen A, et al. Liver fat and lipid oxidation in humans. *Liver Int*. 2009;29(9):1439–1446.

30. Cortez-Pinto H, et al. Alterations in Liver ATP Homeostasis in Human Nonalcoholic SteatohepatitisA Pilot Study. *JAMA*. 1999;282(17):1659–1664.

31. Rector RS, et al. Mitochondrial dysfunction precedes insulin resistance and hepatic steatosis and contributes to the natural history of non-alcoholic fatty liver disease in an obese rodent model. *J Hepatol*. 2010;52(5):727–736.

32. Croci I, et al. Whole-body substrate metabolism is associated with disease severity in patients with non-alcoholic fatty liver disease. *Gut*. 2013;62(11):1625–1633.

33. Moore MP, et al. Compromised hepatic mitochondrial fatty acid oxidation and reduced markers of mitochondrial turnover in human NAFLD. *Hepatol Baltim Md*. 2022;76(5):1452–1465.

34. Moore MP, et al. Relationship Between Serum β-Hydroxybutyrate and Hepatic Fatty Acid Oxidation in Individuals with Obesity and NAFLD. *Am J Physiol-Endocrinol Metab*. 2024;ajpendo.00336.2023.

35. Satapati S, et al. Mitochondrial metabolism mediates oxidative stress and inflammation in fatty liver. *J Clin Invest*. 2015;125(12):4447–4462.

36. Burgess SC, et al. Impaired Tricarboxylic Acid Cycle Activity in Mouse Livers Lacking Cytosolic Phosphoenolpyruvate Carboxykinase. *J Biol Chem*. 2004;279(47):48941–48949.

37. Fu X, et al. Persistent fasting lipogenesis links impaired ketogenesis with citrate synthesis in humans with nonalcoholic fatty liver. *J Clin Invest*;133(9):e167442.

38. Adiels M, et al. Overproduction of large VLDL particles is driven by increased liver fat content in man. *Diabetologia*. 2006;49(4):755–765.

39. Choi SH, Ginsberg HN. Increased very low density lipoprotein (VLDL) secretion, hepatic steatosis, and insulin resistance. *Trends Endocrinol Metab TEM*. 2011;22(9):353–363.

40. Pirazzi C, et al. Patatin-like phospholipase domain-containing 3 (*PNPLA3*) I148M (rs738409) affects hepatic VLDL secretion in humans and *in vitro*. *J Hepatol*. 2012;57(6):1276–1282.

41. Johnson SM, et al. PNPLA3 is a triglyceride lipase that mobilizes polyunsaturated fatty acids to facilitate hepatic secretion of large-sized very low-density lipoprotein. *Nat Commun*. 2024;15(1):4847.

42. Luukkonen PK, et al. Human PNPLA3-I148M variant increases hepatic retention of polyunsaturated fatty acids. *JCI Insight*. 2019;4(16):e127902, 127902.

43. Conboy E, et al. Mitochondrial 3-Hydroxy-3-Methylglutaryl-CoA Synthase Deficiency: Unique Presenting Laboratory Values and a Review of Biochemical and Clinical Features. *JIMD Rep*. 2018;40:63–69.

44. Bouchard L, et al. Mitochondrial 3-hydroxy-3-methylglutaryl-CoA synthase deficiency: clinical course and description of causal mutations in two patients. *Pediatr Res*. 2001;49(3):326–331.

45. Asif S, et al. Hmgcs2-mediated ketogenesis modulates high-fat diet-induced hepatosteatosis. *Mol Metab*. 2022;61:101494.

46. Cotter DG, et al. Ketogenesis prevents diet-induced fatty liver injury and hyperglycemia. *J Clin Invest*. 2014;124(12):5175–5190.

47. Puchalska P, et al. Hepatocyte-Macrophage Acetoacetate Shuttle Protects against Tissue Fibrosis. *Cell Metab*. 2019;29(2):383-398.e7.

48. Queathem ED, et al. Ketogenesis supports hepatic polyunsaturated fatty acid homeostasis via fatty acid elongation. *Sci Adv*. 2025;11(5):eads0535.

49. Ramakrishnan S, et al. Hepatic ketogenesis regulates lipid homeostasis via ACSL1-mediated fatty acid partitioning [preprint]. 2023. https://doi.org/10.21203/rs.3.rs-3147009/v1.

50. Sanyal AJ, et al. Nonalcoholic steatohepatitis: association of insulin resistance and mitochondrial abnormalities. *Gastroenterology*. 2001;120(5):1183–1192.

51. Deja S, et al. Simultaneous tracers and a unified model of positional and mass isotopomers for quantification of metabolic flux in liver. *Metab Eng*. 2020;59:1–14.

52. d'Avignon DA, et al. Hepatic ketogenic insufficiency reprograms hepatic glycogen metabolism and the lipidome. *JCI Insight*. 2018;3(12):e99762, 99762.

53. Stagg DB, et al. Diminished ketone interconversion, hepatic TCA cycle flux, and glucose production in D-β-hydroxybutyrate dehydrogenase hepatocyte-deficient mice. *Mol Metab*. 2021;53:101269.

54. Feola K, et al. Hepatic ketogenesis is not required for starvation adaptation in mice. *Mol Metab*. 2024;86:101967.

55. Alexander M, et al. A diet-dependent host metabolite shapes the gut microbiota to protect from autoimmunity. *Cell Rep*. 2024;43(11). https://doi.org/10.1016/j.celrep.2024.114891.

56. Puchalska P, et al. Determination of ketone bodies in biological samples via rapid UPLC-MS/MS. *Talanta*. 2021;225:122048.

57. Hasenour CM, et al. Mass spectrometry-based microassay of (2)H and (13)C plasma glucose labeling to quantify liver metabolic fluxes in vivo. *Am J Physiol Endocrinol Metab*. 2015;309(2):E191-203.

58. Hughey CC, et al. Loss of hepatic AMP-activated protein kinase impedes the rate of glycogenolysis but not gluconeogenic fluxes in exercising mice. *J Biol Chem*. 2017;292(49):20125–20140.

59. Rome FI, et al. Loss of hepatic phosphoenolpyruvate carboxykinase 1 dysregulates metabolic responses to acute exercise but enhances adaptations to exercise training in mice. *Am J Physiol Endocrinol Metab*. 2023;324(1):E9–E23.

60. Fisher-Wellman KH, et al. Mitochondrial Diagnostics: A Multiplexed Assay Platform for Comprehensive Assessment of Mitochondrial Energy Fluxes. *Cell Rep*. 2018;24(13):3593-3606.e10.

61. Tomoda H, et al. Binding site for fungal beta-lactone hymeglusin on cytosolic 3-hydroxy-3-methylglutaryl coenzyme A synthase. *Biochim Biophys Acta*. 2004;1636(1):22–28.

62. Le Foll C, et al. Regulation of hypothalamic neuronal sensing and food intake by ketone bodies and fatty acids. *Diabetes*. 2014;63(4):1259–1269.

63. Veech RL, et al. The "great" controlling nucleotide coenzymes. *IUBMB Life*. 2019;71(5):565–579.

64. Schmid AI, et al. Liver ATP Synthesis Is Lower and Relates to Insulin Sensitivity in Patients With Type 2 Diabetes. *Diabetes Care*. 2011;34(2):448–453.

65. Felig P, et al. Splanchnic glucose and amino acid metabolism in obesity. *J Clin Invest*. 1974;53(2):582–590.

66. Xu J, et al. Sterol regulatory element binding protein-1 expression is suppressed by dietary polyunsaturated fatty acids. A mechanism for the coordinate suppression of lipogenic genes by polyunsaturated fats. *J Biol Chem*. 1999;274(33):23577–23583.

67. Yahagi N, et al. A crucial role of sterol regulatory element-binding protein-1 in the regulation of lipogenic gene expression by polyunsaturated fatty acids. *J Biol Chem*. 1999;274(50):35840–35844.

68. Botolin D, et al. Docosahexaneoic acid (22:6,n-3) regulates rat hepatocyte SREBP-1 nuclear abundance by Erk- and 26S proteasome-dependent pathways. *J Lipid Res*. 2006;47(1):181–192.

69. Takeuchi Y, et al. Polyunsaturated Fatty Acids Selectively Suppress Sterol Regulatory Element-binding Protein-1 through Proteolytic Processing and Autoloop Regulatory Circuit. *J Biol Chem*. 2010;285(15):11681–11691.

70. Deng X, et al. Docosahexaenoic acid inhibits proteolytic processing of sterol regulatory element-binding protein-1c (SREBP-1c) via activation of AMP-activated kinase. *Biochim Biophys Acta BBA - Mol Cell Biol Lipids*. 2015;1851(12):1521–1529.

71. Green CJ, et al. Hepatic de novo lipogenesis is suppressed and fat oxidation is increased by omega-3 fatty acids at the expense of glucose metabolism. *BMJ Open Diabetes Res Care*. 2020;8(1):e000871.

72. Malloy CR, et al. Contribution of various substrates to total citric acid cycle flux and anaplerosis as determined by 13C isotopomer analysis and O2 consumption in the heart. *Magma N Y N*. 1996;4(1):35–46.

73. Postic C, et al. Dual Roles for Glucokinase in Glucose Homeostasis as Determined by Liver and Pancreatic β Cell-specific Gene Knock-outs Using Cre Recombinase*. *J Biol Chem*. 1999;274(1):305–315.

74. Horton JL, et al. The failing heart utilizes 3-hydroxybutyrate as a metabolic stress defense. *JCI Insight*. 2019;4(4):e124079, 124079.

75. Tr K, et al. Pyruvate-supported flux through medium-chain ketothiolase promotes mitochondrial lipid tolerance in cardiac and skeletal muscles. *Cell Metab*. 2023;35(6). https://doi.org/10.1016/j.cmet.2023.03.016.

Tables

Table 1. MASLD-MASH Patient Characteristics

Table summarizing the human cohort studied encompassing markers of sex, age, body composition, systemic glucose homeostasis, and liver health.

| Human Cohort Characteristics		Average	±SD
Sex and Age	Sex (F/M)	15 / 1	na
	Age (years old)	48	14
Body Composition	Body Weight (kg)	112	18
	Body Mass Index (BMI) (kg/m2)	42	6
	Body Fat (% from DXA)	51	4
	Android Fat (% from DXA)	59	4
	Gynoid Fat (% from DXA)	51	6
	Lean Body Mass (LBM) (% from DXA)	47	4
	Bone Mineral Density (g/cm2)	1.3	0.2
Glucose Homeostasis	Fasting Blood Glucose (mg/dL)	104	13
	Fasting Insulin (U/L)	27	11
	HOMA-IR	6.7	2.6
	HbA1c (%)	5.8	0.5
	Insulin Sensitivity (SI) ((mU/L)-1 min-1)	3.8	8.1
	Acute Insulin Response to Glucose (AIRg) ((mU/L) min-1)	851	843
	Disposition Index (DI) (SI x AIRg) (unitless)	1294	1056
	Glucose Effectiveness (Sg) x10-2 (min-1)	1.2	0.5
	Glucose Effectiveness at Zero Insulin (GEZI) x10-2 (min-1)	0.4	1.7
	Beta-cell Function (mU/L)	378	226
	Insulin Resistance	5.9	2.2
Liver Function	Alanine Transaminase (ALT) (U/L)	50.3	16.7
	Aspartate Aminotransferase (AST) (U/L)	32.9	17.7
	Albumin (g/dL)	3.9	0.3
	Alkaline Phosphatase (ALP) (U/L)	95.4	20.9
	Bilirubin (mg/dL)	0.5	0.3

Figures and Figure Legends
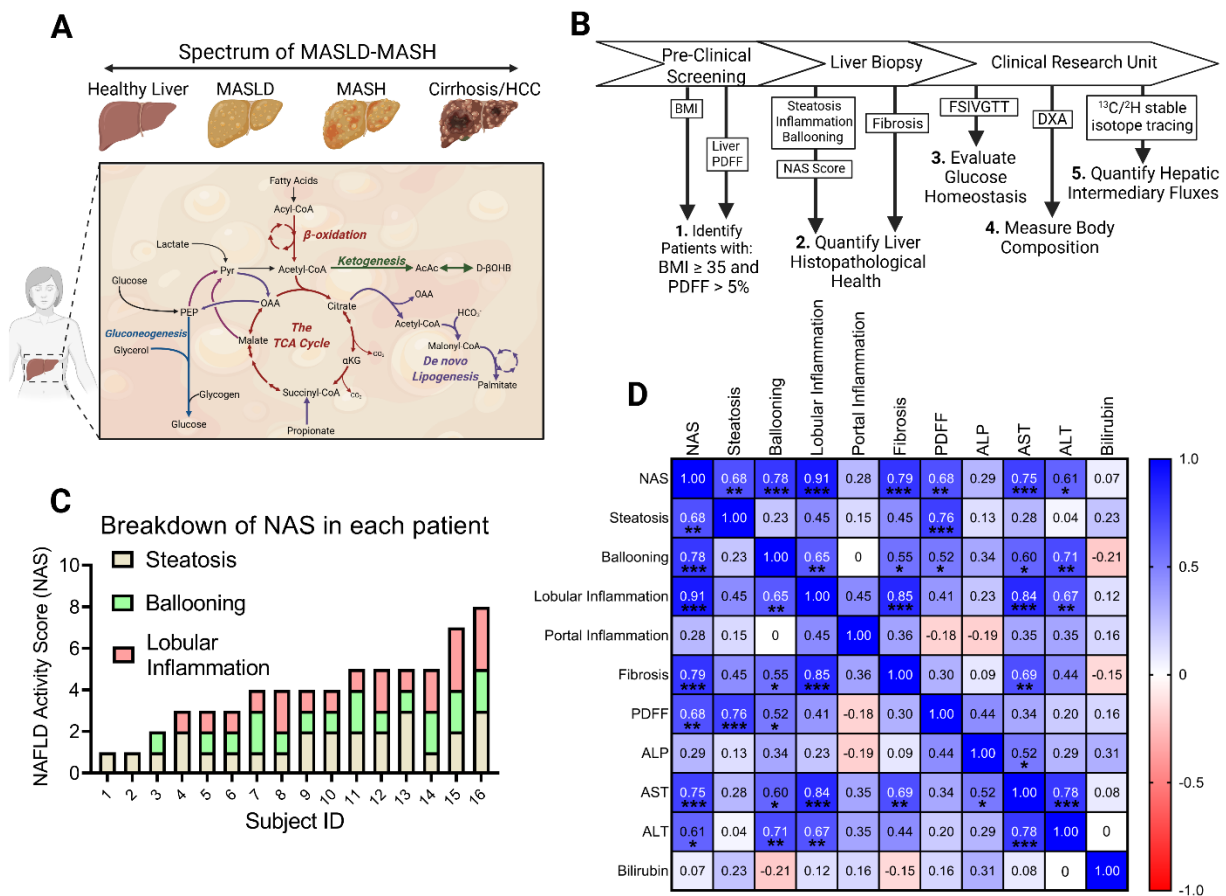
Figure 1. Metabolic characteristics of MASLD-MASH. (A) The initial stages of metabolic dysfunction-associated steatotic liver disease (MASLD) begins with hepatic steatosis, linked to accelerations in: de novo lipogenesis (DNL), turnover of the tricarboxylic acid (TCA) cycle, and phosphoenolpyruvate (PEP)-derived gluconeogenesis (GNG). Metabolic shifts during the progression of MASLD to metabolic dysfunction-associated steatohepatitis (MASH) remain poorly understood. **(B)** Study design. Patients with body mass index (BMI) ≥ 35 and liver proton density fat fraction (PDFF) > 5% underwent a liver biopsy, FSIVGTT, and DXA imaging. After an overnight fast, eight hepatic intermediary metabolic fluxes were quantified using ^{2}H/^{13}C stable-isotope tracing. **(C)** Distributions of the NAFLD activity scores (NAS) in all 16 participants (15 female, 1 male). **(D)** Correlation matrix of NAS score with histological scores for steatosis,

ballooning, inflammation, fibrosis, PDFF, liver enzymes and bilirubin. Pearson correlations

coefficients (r) are shown in heat map format with the magnitude of the correlation given by the

right-hand legend and displayed in each square. Correlations were accepted as significant if

$p<0.05$ and are shown in each box as indicated, * $p<0.05$, ** $p<0.01$, ***$p<0.001$.

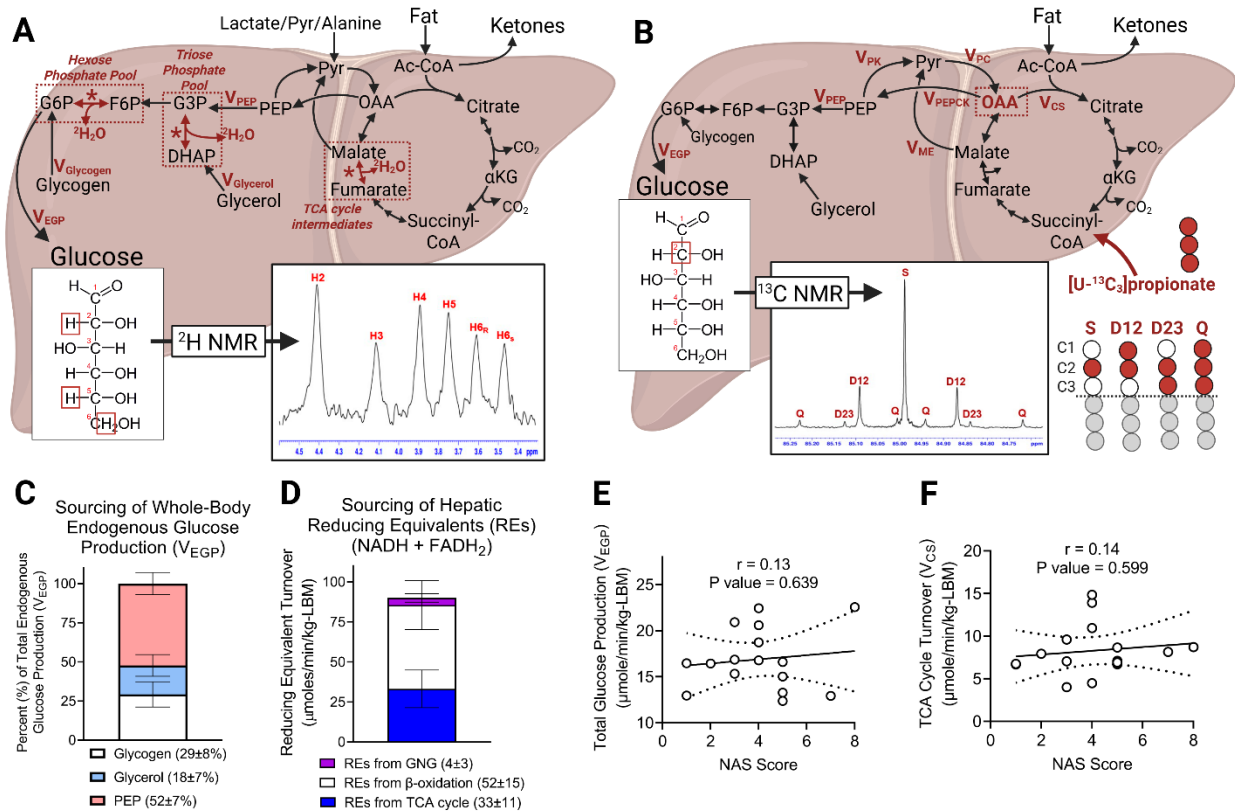**Figure 2. Liver injury does not correlate with endogenous glucose production or TCA cycle turnover.** Fluxes through hepatic intermediary metabolic pathways were quantified in humans following oral administration of heavy water (^2H_2O) and [U-$^{13}C_3$]propionate. [3,4-$^{13}C_2$]glucose and D-[U-$^{13}C_4$]βOHB were intravenously infused allowing whole body glucose (V_{EGP}) and βOHB turnover ($V_{RaβOHB}$) to be quantified at metabolic and isotopic steady state. **(A)** Fractional sourcing of glucose can be quantified from the ^2H enrichment pattern of plasma glucose using ^2H NMR, which by multiplying by V_{EGP}, allows absolute reaction velocities (V) (i.e., flux) for hepatic glucose sourcing pathways to be quantified. **(B)** Administration of [U-$^{13}C_3$]propionate ^{13}C-enriches TCA cycle intermediates, which sources phosphoenolpyruvate (PEP). Using ^{13}C NMR, and the multiplet arising from the C2 resonance of plasma glucose, the resulting metabolic network models oxidative and anaplerotic nodes of the TCA cycle in parallel to glucose production. By normalizing fluxes to V_{PEP}, the absolute reaction velocities of the TCA cycle, anaplerosis/cataplerosis, and pyruvate cycling can be quantified. **(C)** Average percent of

V_{EGP} derived from glycogen, glycerol, and PEP, highlighting that TCA cycle-sourced PEP is the major contributor to V_{EGP} in the fasted state in humans. **(D)** Average reducing equivalents (REs) derived from GNG, β-oxidation and the TCA cycle. The correlations of NAS score with **(E)** V_{EGP} and **(F)** TCA cycle turnover (V_{CS}). Data are expressed as either mean ± standard deviation or shown as correlations. Pearson correlations coefficients (r) are shown on each group along with a line of best fit and 95% confidence intervals calculated using linear regression. Correlations were accepted as significant if $p<0.05$. P values are shown on each graph.
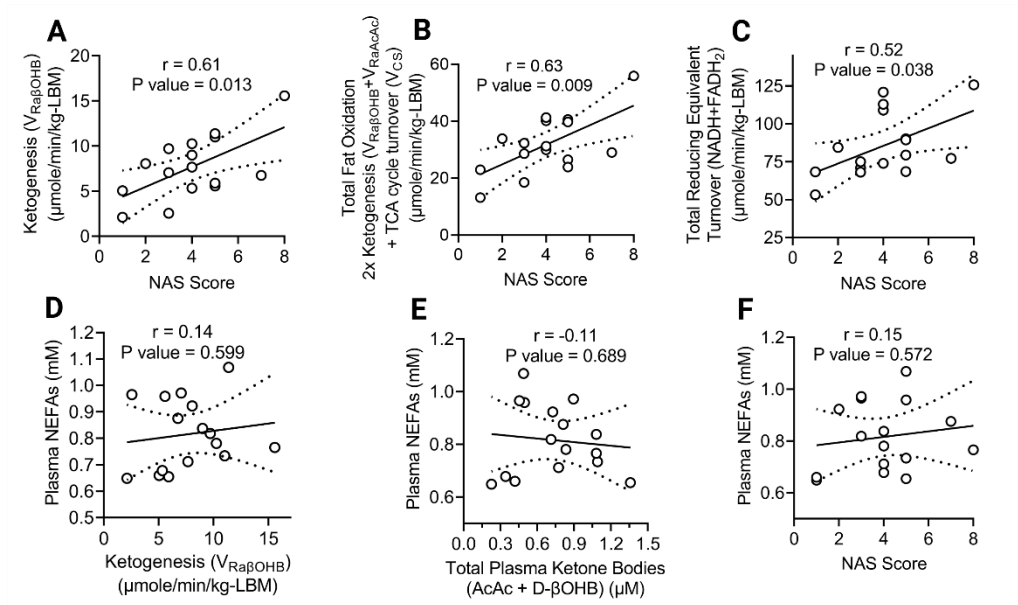
Figure 3. Liver injury correlates with endogenous ketogenesis and hepatic fat oxidation.
The correlation of NAS with **(A)** endogenous ketogenesis ($V_{Ra\beta OHB}$), **(B)** total fat oxidation, and **(C)** total RE turnover. Correlation of serum non-esterified fatty acid (NEFA) concentrations with **(D)** endogenous ketogenesis ($V_{Ra\beta OHB}$), **(E)** total plasma ketone bodies (AcAc + βOHB), and **(F)** NAS score. Pearson correlations coefficients (r) are given on each graph along with a line of best fit calculated using linear regression. Correlations were accepted as significant if p<0.05. P values are shown on each graph.
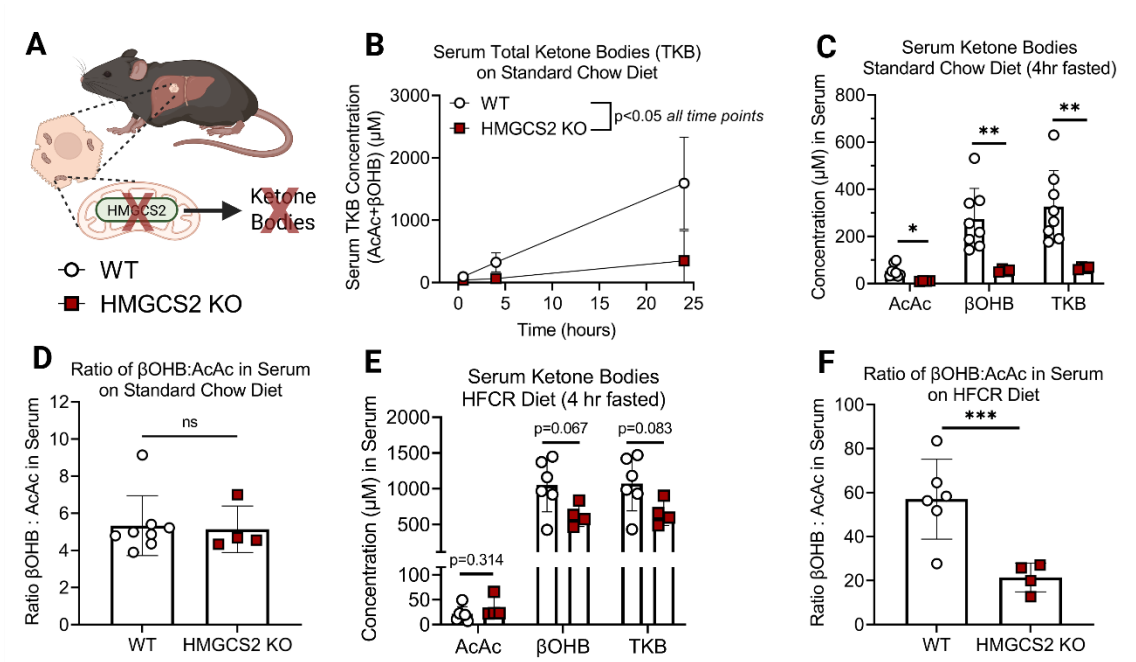
Figure 4. Loss of hepatocyte HMGCS2 impairs fasting ketosis. (A) Ketogenesis-null mice were generated by deleting the gene encoding 3-hydroxymethylglutaryl-CoA synthase 2 (HMGCS2) in hepatocytes. Littermate control (wild-type, WT) and HMGCS2 hepatocyte-specific knock out (HMGCS2-Liver-KO) male and female mice were maintained on standard chow diet, switched to a high-fat carbohydrate-restricted (HFCR) diet for 1 week, and studied in the random-fed or fasted state. **(B)** Functional loss of HMGCS2 was confirmed in vivo in chow-fed mice by demonstrating HMGCS2-Liver-KO mice failed to increase fasting total ketone bodies (TKB), **(C)** marked by a decrease in both AcAc and βOHB (4h fasted) (n=4-8/group). **(D)** Ratio of βOHB:AcAc in 4h fasted WT and HMGCS2-Liver-KO mice fed chow diet (n=4-8/group). **(E)** Serum TKB analysis of WT and HMGCS2-Liver-KO mice fed HFCR-diet (n=4-6/group). **(F)** The ratio of βOHB:AcAc in WT and HMGCS2-Liver-KO mice fed HFCR-diet (n=4-6/group). Data are expressed as mean ± standard deviation. Statistical differences were determined by Student's t-tests and accepted as significant if $p<0.05$. * $p<0.05$, ** $p<0.01$, ***$p<0.001$, as indicated. NS = not statistically significant.
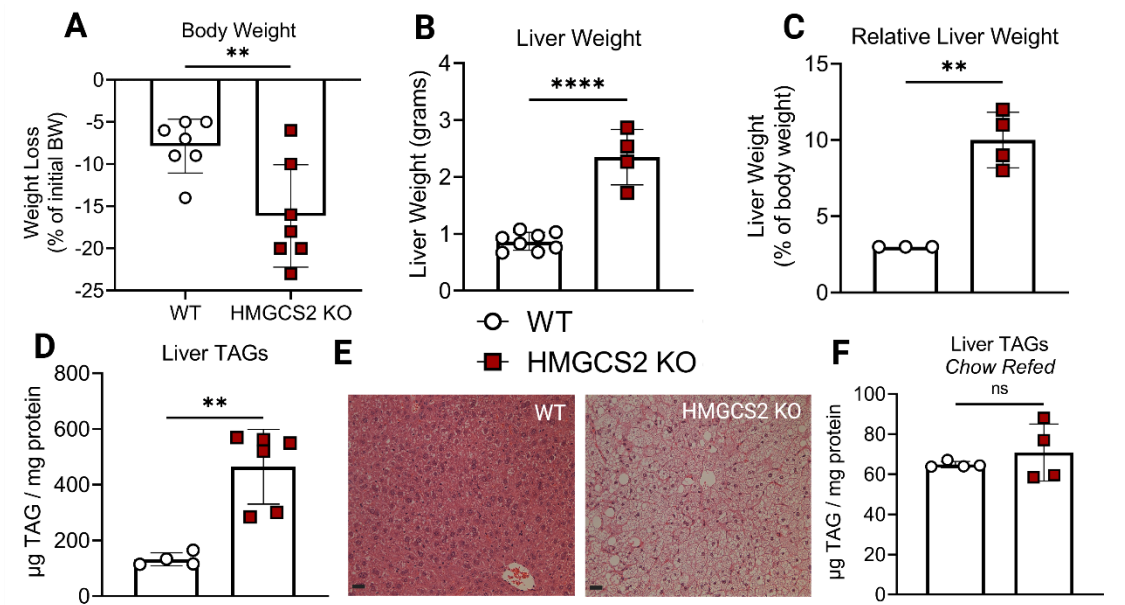
Figure 5. Ketogenic insufficiency induces hepatomegaly and steatosis. Littermate control (WT) and HMGCS2-Liver-KO male and female mice maintained on standard chow diet were switched to HFCR diet for 1 week. **(A)** Net change in body weight after switching diets (n=7/group). **(B)** Total liver weight (grams), and **(C)** relative liver weight (% of body weight) (n=3-8/group). Total liver triacylglycerols (TAG) in random-fed livers quantified **(D)** colorimetrically and shown **(E)** histologically with H&E stain. **(F)** Total liver TAGs in HFCR diet-fed mice, after 1 week of refeeding standard chow (n=4/group). Data are expressed as mean ± standard deviation. Scale bar in H&E images are 25 μm. Statistical differences were determined by Student's t-tests and accepted as significant if p<0.05. ** p<0.01, ****p<0.0001, as indicated. NS = not statistically significant.
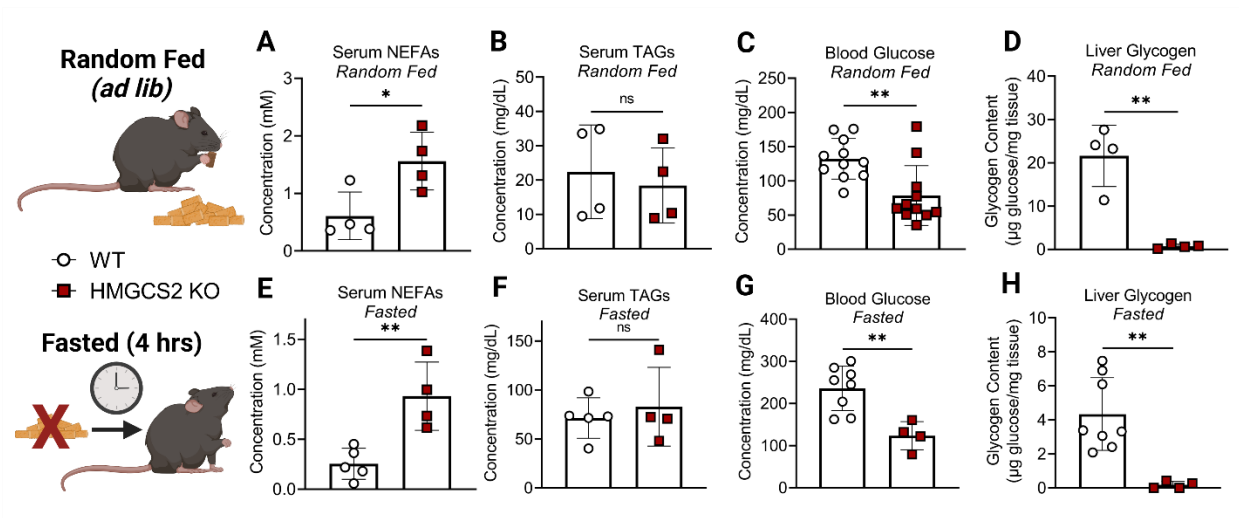
Figure 6. Ketogenic insufficiency induces relative hypoglycemia in HFCR diet-fed mice.

Systemic physiological markers of whole-body metabolism in **(A-D)** random-fed and **(E-H)** 4h fasted male and female littermate control (WT) and HMGCS2-Liver-KO mice, including: blood non-esterified fatty acids (NEFAs), TAGs, and glucose. Also included is total liver glycogen content (n=4-11/group). Data are expressed as mean ± standard deviation. Statistical differences were determined by Student's t-tests and accepted as significant if p<0.05. * p<0.05, ** p<0.01, ***p<0.001, as indicated. NS = not statistically significant.
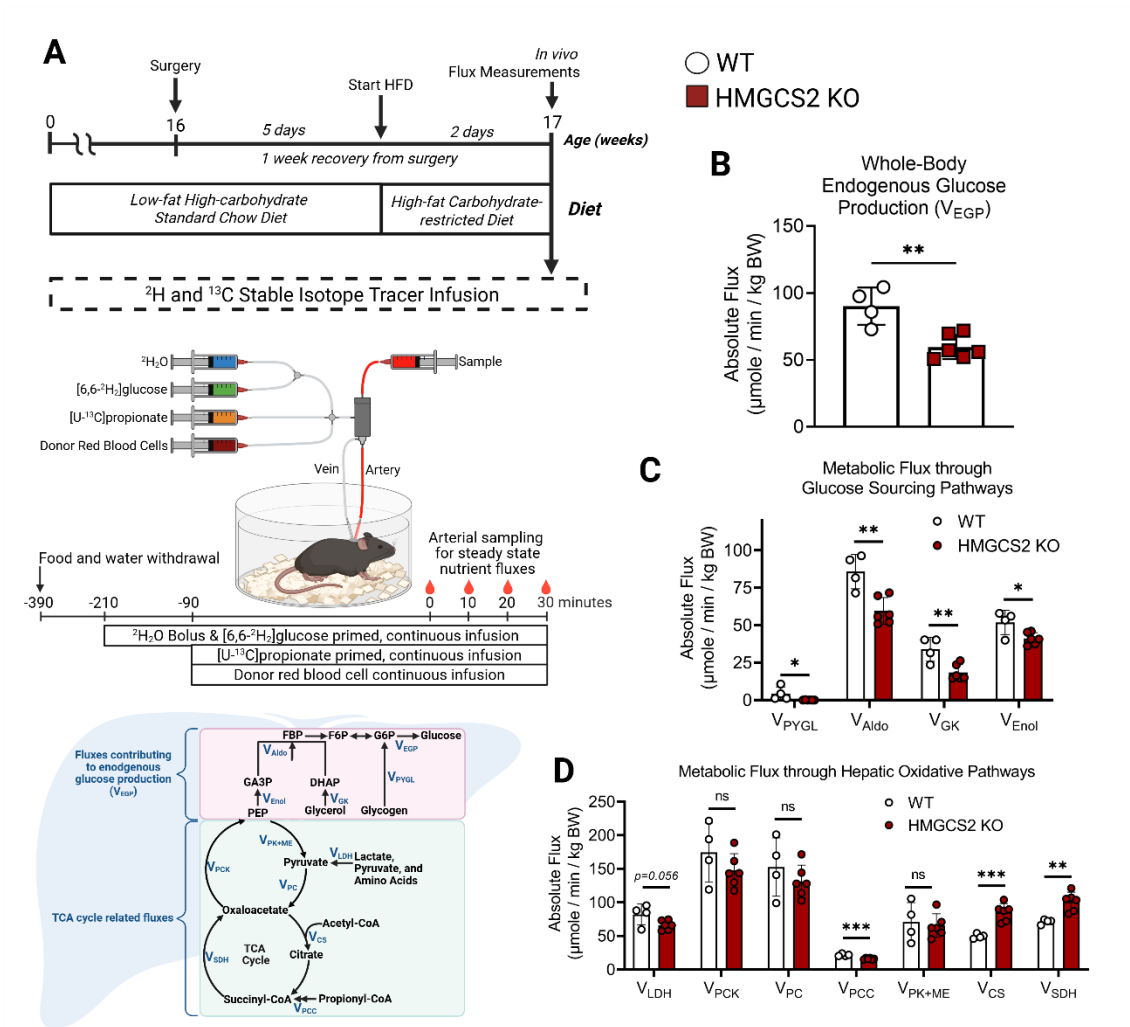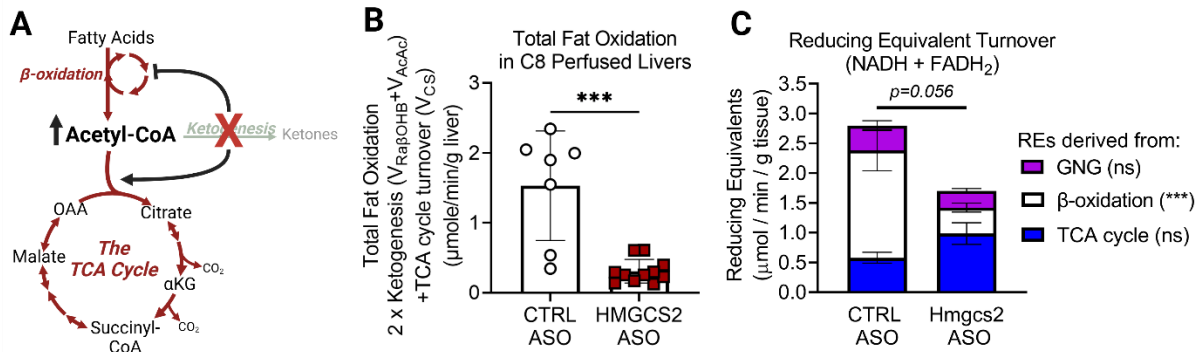
Figure 7. Ketogenic insufficiency diminishes gluconeogenesis in mice. (A) Overview of in vivo hepatic flux modeling study design. (Top) Fluxes were measured in female littermate control (WT) and HMGCS2-Liver-KO mice. Five days after surgical implantation of indwelling catheters mice were switched from standard chow to a HFCR diet, then fluxes were measured after a two-day acclimation period. (Middle) Stable isotope tracers were administered including [6,6-^{2}H$_2$]glucose, [U-^{13}C$_3$]propionate, and heavy water (^{2}H$_2$O). Red blood cells from donor mice were infused to maintain hematocrit. Samples collected for analysis are during the final 30 minutes after metabolic and isotopic steady-state has been reached. (Bottom) Diagram of reaction velocities (V) (i.e., fluxes) modeled using a mass isotopomer distribution analysis of derivatized plasma glucose acquired via GC-MS. **(B)** Rates of whole-body endogenous glucose

production (V_{EGP}) as measured via tracer dilution of [6,6-$^2H_2$]glucose (n=4-6/group). **(C)** Absolute rates of glucose sourcing pathways including: glycogenolysis (V_{PYGL}), total gluconeogenesis (V_{Aldo}), and rates of glycerol (V_{GK}) and phosphoenolpyruvate (PEP) (V_{Enol}) flux to glucose (n=4-6/group). **(D)** Absolute rates for reactions in the oxidative flux network shown in panel A including: lactate dehydrogenase (LDH, V_{LDH}), PEP carboxykinase (PCK) (V_{PCK}, i.e., total TCA cycle cataplerosis), anaplerosis into the TCA cycle via pyruvate carboxylase (PC, V_{PC}), or via propionyl-CoA carboxylase (PCC, V_{PCC}), pyruvate cycling as the sum of pyruvate kinase (PK) and malic enzyme (ME) (V_{PK+ME}), citrate synthase (CS) flux (V_{CS}, i.e., TCA cycle turnover) and succinate dehydrogenase (SDH) flux (V_{SDH}, n=4-6/group). Data are expressed as mean ± standard deviation. Statistical differences were determined by Student's t-tests and accepted as significant if $p<0.05$. * $p<0.05$, ** $p<0.01$, ***$p<0.001$, as indicated. NS = not statistically significant.

Chow Diet-fed Perfused Livers

A Fatty Acids, β-oxidation, ↑Acetyl-CoA, Ketogenesis ✕ Ketones, OAA, Citrate, Malate, The TCA Cycle, αKG, CO_2, Succinyl-CoA, CO_2

B Total Fat Oxidation in C8 Perfused Livers — Total Fat Oxidation $2 \times$ Ketogenesis ($V_{R_{\alpha}\beta OHB} + V_{AcAc}$) + TCA cycle turnover ($V_{CS}$) (µmole/min/liver); ***; CTRL ASO, HMGCS2 ASO

C Reducing Equivalent Turnover (NADH + FADH$_2$) — Reducing Equivalents (µmol / min / g tissue); $p=0.056$; REs derived from: GNG (ns), β-oxidation (***), TCA cycle (ns); CTRL ASO, Hmgcs2 ASO

Western Diet-fed Perfused Livers

D Hepatic TCA Cycle Turnover — µmol / min / g liver; *; CTRL ASO, Hmgcs2 ASO

E Total Fat Oxidation in C8 Perfused Livers — Total Fat Oxidation $2 \times$ Ketogenesis ($V_{R_{\alpha}\beta OHB} + V_{AcAc}$) + TCA cycle turnover ($V_{CS}$) (µmoles/min/g liver); **; CTRL ASO, HMGCS2 ASO

F Reducing Equivalent Turnover (NADH + FADH$_2$) — Reducing Equivalents (µmol / min / g tissue); $p=0.090$; REs derived from: GNG (ns), β-oxidation (**), TCA cycle ($p=0.0504$); CTRL ASO, Hmgcs2 ASO
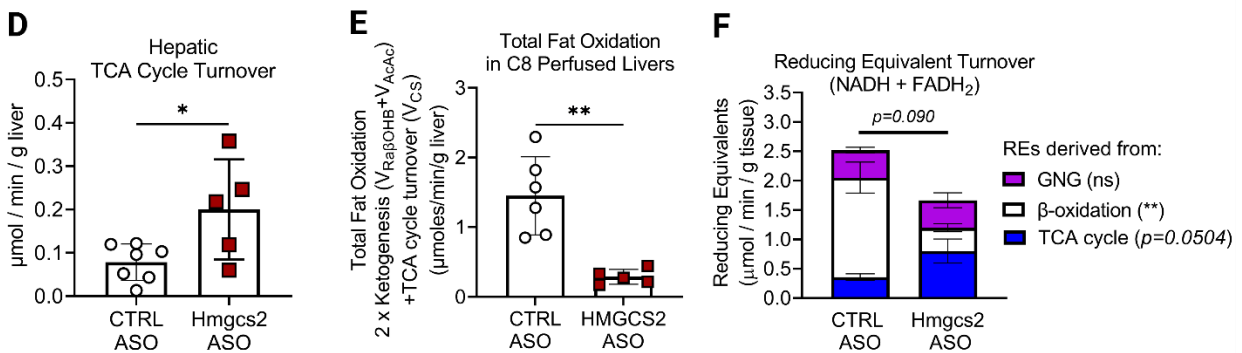
Figure 8. Ketogenic insufficiency impairs fat oxidation in perfused livers. (A) Prior studies have demonstrated that ketogenesis-insufficiency induced by loss of HMGCS2 causes accumulation of mitochondrial acetyl-CoA and acceleration of the TCA cycle. Livers of male mice treated with scrambled control antisense oligonucleotide (ASO) or mouse *Hmgcs2* ASO were perfused with octanoate (C8) and oxidative fluxes quantified using ^{2}H/^{13}C stable isotope tracing. **(B)** Total fat oxidation quantified as the summation of (2 x ketogenesis) + TCA cycle turnover, and **(C)** reducing equivalent (RE) turnover (NADH + FADH$_2$) broken down into REs from gluconeogenesis (GNG), β-oxidation, and the TCA cycle, in perfused livers from control and *Hmgcs2* ASO mice on chow diet (n=10-11/group). Fat oxidation was also studied in ex vivo C8 perfused livers of control and *Hmgcs2* ASO-treated mice maintained on a 42% high-fat high-sucrose Western diet (WD) for 8 weeks. **(D)** TCA cycle turnover, **(E)** total fat oxidation, and **(F)** RE production rate (NADH + FADH$_2$) in perfused livers from control and *Hmgcs2* ASO-treated mice on WD (n=5-6/group). Data are expressed as mean ± standard deviation. Statistical

differences were determined by Student's t-tests or two-way ANOVA and accepted as significant if $p<0.05$. * $p<0.05$, ** $p<0.01$, ***$p<0.001$, as indicated. NS = not statistically significant.
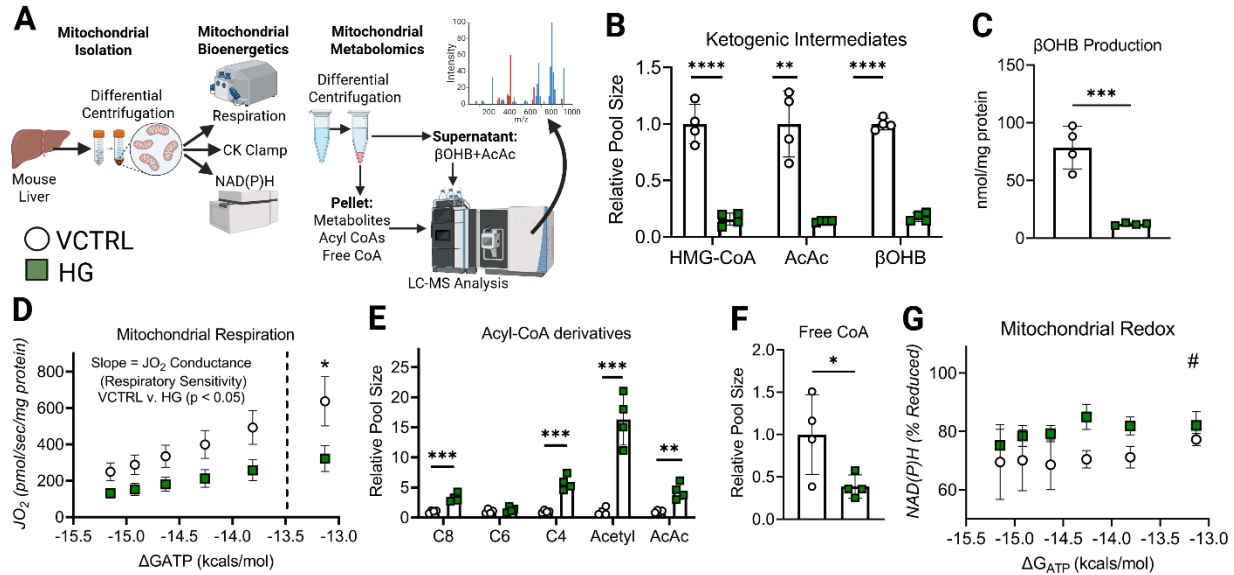
Figure 9. Ketogenic insufficiency impairs fat oxidation in isolated mitochondria. (A)
Mitochondrial Diagnostics Workflow. Liver mitochondria isolated by differential centrifugation
and fueled by palmitoyl-L-carnitine + α-ketoglutarate, were used to assess the effects of
hymeglusin (HG, HMGCS inhibitor) versus vehicle control (VCTRL) on βOHB production,
respiratory kinetics, and redox potential during a creatine kinase (CK) energetic clamp, and on
metabolite abundance post-CK clamp. **(B)** Relative abundance of 3-hydroxymethylglutaryl-CoA
(HMG-CoA), AcAc and βOHB in mitochondria, and **(C)** βOHB production measured in
supernatant collected post-CK clamp (n=4/group). **(D)** Respiration (JO_2) plotted as a function of
energy demand [ΔG_{ATP} (kcal/mol)], with respiratory sensitivity (i.e., JO_2 conductance) measured
as the slope of the curve (n=4/group). Results of Student's t-test of slopes between VCTRL and
HG is shown on the graph. **(E)** Relative abundance of acyl-CoA species, and **(F)** free coenzyme
A in mitochondria (n=4/group). **(G)** Redox potential [(NAD(P)H % reduction) plotted as a
function of energy demand (ΔG_{ATP} (kcals/mol), n=4/group)]. Pool sizes are from mitochondria
after incubation at a fixed energy demand (ΔG_{ATP} = -14.26 kcals/mol). Data are expressed as
mean ± standard deviation. Statistical differences were determined by Student's t-tests or two-
way ANOVA and accepted as significant if $p<0.05$. * $p<0.05$, ** $p<0.01$, ***$p<0.001$, as
indicated. # = significant by 2-way ANOVA ($p <0.05$). NS = not statistically significant.
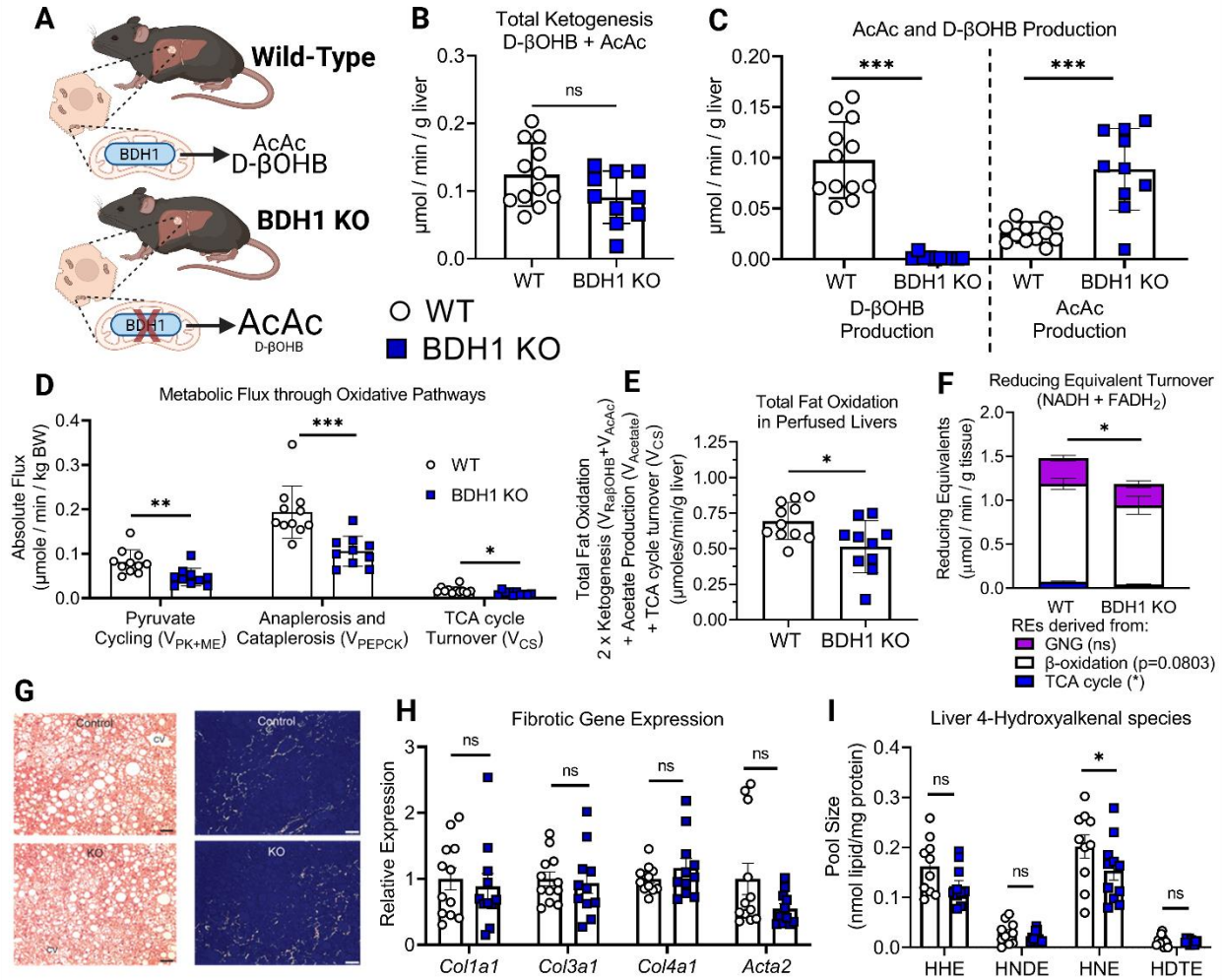
Figure 10. Loss of hepatocyte BDH1 impairs total hepatic fat oxidation but does not exacerbate HFD-induced liver fibrosis. (A) Male hepatocyte-specific BDH1-null (BDH1-Liver-KO) and littermate control (WT) mice were maintained on standard chow diet then were switched to a 42% high-fat high-sucrose WD for 16 weeks, after which oxidative fluxes were studied in long-chain fatty acid (LCFA) ex vivo perfused livers. **(B)** Total ketone body production, and **(C)** AcAc and βOHB production, in livers of WT and BDH1-Liver-KO mice (n=10-11/group). **(D)** Absolute rates of oxidative pathways including: pyruvate cycling (V_{PK+ME}), total anaplerosis and cataplerosis (V_{PEPCK}), and TCA cycle turnover (V_{CS}) (n=10-11/group). **(E)** Total fat oxidation calculated at (2 x ketogenesis) + acetogenesis + TCA cycle turnover, and **(F)** reducing equivalent (RE) turnover (NADH + $FADH_2$) broken down into RE's generated from

gluconeogenesis (GNG), β-oxidation, and the TCA cycle (n=10-11/group). **(G)** Liver H&E and

picrosirius red histological staining, **(H)** gene expression for fibrotic gene markers, and **(I)**

absolute levels of lipid peroxide 4-hydroxyalkenal species in livers of WT and BDH1-Liver-KO

mice maintained on 42% kcal fat WD (n=10-12/group). Scale bar in H&E images are 25 µm.

Scale bar for picrosirius red images are 100 µm. Data are expressed as mean ± standard

deviation. Statistical differences were determined by Student's t-tests and accepted as

significant is $p < 0.05$. * $p < 0.05$, ** $p < 0.01$, ***$p < 0.001$, as indicated. NS = not statistically

significant.